Title

Changes in geophysical properties caused by fluid injection into porous rocks: analytical models

Journal

Geophysical Prospecting, 65(3)

ISSN

0016-8025

Authors

Pride, Steven R
Berryman, James G
Commer, Michael
et al.

Publication Date

2017-05-01

DOI

10.1111/1365-2478.12435

Peer reviewed

Geophysical Prospecting

EAGE EUROPEAN ASSOCIATION OF GEOSCIENTISTS & ENGINEERS

Geophysical Prospecting, 2016 doi: 10.1111/1365-2478.12435

Changes in geophysical properties caused by fluid injection into porous rocks: analytical models

Steven R. Pride*, James G. Berryman, Michael Commer, Seiji Nakagawa, Gregory A. Newman and Donald W. Vasco

Lawrence Berkeley National Laboratory, Energy Geosciences Division, 1 Cyclotron Road, MS 74R-316C, Berkeley, CA 94720, USA

Received September 2015, revision accepted June 2016

ABSTRACT

Analytical models are provided that describe how the elastic compliance, electrical conductivity, and fluid-flow permeability of rocks depend on stress and fluid pressure. In order to explain published laboratory data on how seismic velocities and electrical conductivity vary in sandstones and granites, the models require a population of cracks to be present in a possibly porous host phase. The central objective is to obtain a consistent mean-field analytical model that shows how each modeled rock property depends on the nature of the crack population. The crack populations are described by a crack density, a probability distribution for the crack apertures and radii, and the averaged orientation of the cracks. The possibly anisotropic nature of the elasticity, conductivity, and permeability tensors is allowed for; however, only the isotropic limit is used when comparing to laboratory data. For the transport properties of conductivity and permeability, the percolation effect of the crack population linking up to form a connected path across a sample is modeled. However, this effect is important only in crystalline rock where the host phase has very small conductivity and permeability. In general, the importance of the crack population to the transport properties increases as the host phase becomes less conductive and less permeable.

Key words: Seismic velocities, Electrical conductivity, Permeability, Effective stress, Fluid flow, Anisotropy.

1 INTRODUCTION

Fluid injected into the subsurface from a borehole alters the physical and chemical state of the Earth. As part of an ongoing research project, we are interested in developing methods to monitor such alterations using time-lapse geophysical data such as seismic and electromagnetic measurements. This paper is concerned with the development of analytical models for use in the inverse problem that describe how the pertinent geophysical properties change as a result of fluid injection.

The injected fluid mass compresses the surrounding rock and causes the stress tensor to change, falling off as r^{-2} with distance r from the injection point in the borehole. As the fluid diffuses out into the formation, additional changes in the pore pressure take place once the injected-fluid front arrives at a given voxel under consideration. The induced stress and fluid-pressure changes near the borehole will likely not exceed the 10 MPa level in most industrial applications (which is the order of the tensile strength of sandstones). Fluid injection alters the physical properties of a given voxel through four mechanisms: (i) the injected fluid has different physical properties than the *in situ* fluid (so-called "fluid substitution"); (ii) the changing pore pressure and stress fields cause already existing cracks and fractures to further open (elastically soften) or close (elastically stiffen); (iii) the changing pore pressure and stress fields cause new cracks and fractures to arrive

*E-mail: srpride@lbl.gov

once effective-stress thresholds (or criteria) are met; and (iv) over longer timescales, the altered chemical equilibrium can provoke precipitation or dissolution of minerals. The main focus of this study is on the effect of stress and pore pressure on the physical properties; however, we also address fluid substitution effects for the specific case of a brine of one salinity replacing a brine of a different salinity.

We specifically want to obtain explicit analytical models for how the seismic velocities, porosity, electrical conductivity, and fluid-flow permeability vary with effective stress using the same rock description for all the geophysical properties. The proposed models allow for how stress-induced damage in the form of evolving crack populations alter the geophysical properties, but they do not address the stress thresholds for when such new damage enters a voxel in the Earth.

There is a wealth of models in the literature (e.g., Wyble 1958; Cheng and Toksöz 1979; Zimmerman, Sommerton, and King 1986; Kaselow and Shapiro 2004; Daley *et al.* 2006; Liu, Rutqvist, and Berryman 2009; Zhang, Sayer, and Adachi 2009; Liu, Wei, and Rutqvist 2013) designed to describe the effective-stress dependence of rock properties. Like most authors before us, in order to account for the rather large variations of the elastic moduli of rocks observed in laboratory effective-stress experiments, we find it necessary to introduce a population of compliant cracks into a possibly porous host material. Of the many theories available for the elastic moduli of dry cracked rocks, the simplest approach is that of Sayers and Kachanov (1995) in which the interaction between cracks is entirely neglected and the effective rock compliance is linear in crack density, i.e., the stress is taken to be uniform throughout a rock sample, and the total strain produced by each crack and the host phase is simply added up. This is the approach adopted here as well. Grechka and Kachanov (2006a, b) have demonstrated numerically that when cracks are closely spaced and even intersecting, the non-interaction approximation still works well. This is due to the cancelling stress fields emanating from randomly oriented cracks. The equivalent mean-field theory for how cracks influence permeability was developed by Oda (1985). In the present work, we develop a unified treatment of elastic moduli, electrical conductivity, and permeability using the non-interacting crack approximation and using the same parameters to describe the crack population for each property. For the transport properties (permeability and electrical conductivity), we further allow for the crack-phase percolation that takes place at sufficiently large crack densities. In the case of an impermeable and insulating host material, allowing for such crack percolation is important. In the case of cracks embedded into a permeable and conducting host material, the crack percolation effect is shown here to be much less important and often negligible. We show that the models developed here are capable of predicting published laboratory data. In the comparisons to lab data, we restrict ourselves to determining isotropic properties. However, in the model development, we allow the crack populations to create anisotropy.

In Section 2, we review poroelasticity and give the famous fluid substitution result of Gassmann (1951) for how the undrained stiffness tensor depends on the drained stiffness tensor in a material with an anisotropic porespace. We then obtain effective-stress models for the drained elastic moduli (Section 3), the porosity, the formation factor, and permeability (Section 4). In Section 5, the geophysical properties of seismic velocities and electrical conductivity, as well as the permeability and porosity, are compared with published laboratory data as a function of effective stress.

2 POROELASTICITY

Poroelasticity (e.g., Biot 1956; Biot and Willis 1957) provides a general context for understanding how evolving fluid pressure and/or fluid substitution influences the geophysical properties.

Isotropic poroelastic constitutive laws relate the total time derivatives of the stress tensor $\boldsymbol{\tau}$ and fluid pressure P to the strain rate of a sample $\nabla\mathbf{v}$ (where $\mathbf{v}$ is the average velocity of the solid grains in a voxel of porous material) and rate of fluid accumulation $\nabla\cdot\mathbf{q}$ (where $\mathbf{q}$ is the Darcy velocity across the voxel) as

$$\frac{\partial\boldsymbol{\tau}}{\partial t}=[K_u\nabla\cdot\mathbf{v}+\alpha M\nabla\cdot\mathbf{q}]\,\mathbf{I}+\mu\left[\nabla\mathbf{v}+(\nabla\mathbf{v})^T-\frac{2}{3}\nabla\cdot\mathbf{v}\,\mathbf{I}\right], \tag{1}$$

$$-\frac{\partial P}{\partial t}=M[\alpha\nabla\cdot\mathbf{v}+\nabla\cdot\mathbf{q}], \tag{2}$$

where $\mathbf{I}$ is the identity tensor. Formally, there should be an advective derivative on the left-hand side of these laws, but it can be shown to be completely negligible for all of our applications. These differential laws allow for non-linear elasticity in that the elastic moduli may be varying in time. One of our primary goals for this paper is to provide rules and formulas for how the elastic moduli vary.

The elastic moduli in the above are defined as follows:

$$K_u=K_d+\alpha^2M, \tag{3}$$

$$\alpha = \frac{1 - K_d/K_u}{B}, \tag{4}$$

$$M = \frac{BK_u}{\alpha}, \tag{5}$$

where K_u is the undrained bulk modulus (bulk modulus of a sealed sample), B the Skempton's coefficient (ratio of fluid pressure to confining pressure for a sealed sampled), K_d the drained (or dry) bulk modulus that is independent of the fluid type in the pores, and μ the drained (or dry) shear modulus. These moduli will vary with time due to the deformation of the pore space as modelled herein and due to fluid substitution effects (with the exception of μ, which is independent of the fluid's presence).

The Gassmann (1951) fluid substitution relations hold whenever the solid grains are well modelled as being isotropic and homogeneous throughout each sample, and are given by

$$B = \frac{1 - K_d/K_s}{1 - K_d/K_s + \phi(K_d/K_f - K_d/K_s)}. \tag{6}$$

$$K_u = \frac{K_d}{1 - B(1 - K_d/K_s)}. \tag{7}$$

Using (7) in (4) yields $\alpha = 1 - K_d/K_s$. The Gassmann relations tell us how K_u and B depend on the drained bulk modulus $K_d(\boldsymbol{\tau}, P)$, the fluid bulk modulus $K_f(P)$, the solid bulk modulus K_s, and porosity $\phi(\boldsymbol{\tau}, P)$. When fluid substitution is occuring at constant stress, only the fluid bulk modulus is changing, and this is why the Gassmann relations are referred to as fluid substitution relations. What is needed next are specific models that allow both K_d and μ (the bulk and shear moduli of drained/dry samples) to vary in time either explicitly with effective stress or as porosity changes.

Before addressing this question, we pause to recall the more general result of Gassmann (1951) for how the undrained elastic stiffness tensor C^u_{ijkl} depends on the drained elastic stiffness tensor C^d_{ijkl} of an anisotropic porous material. In this model, it is again assumed that the solid framework of grains is made of an isotropic mineral of stiffness K_s and that all anisotropy is due to the shape and orientation of the connected pores and/or cracks. The result is

$$C^u_{ijkl} = C^d_{ijkl} + \frac{K_s\,\alpha_{ij}\alpha_{kl}}{\alpha_{pp}/3 - \phi(1 - K_s/K_f)} \quad \text{when } i = j \text{ and } k = l, \tag{8}$$

$$C^u_{ijkl} = C^d_{ijkl} \quad \text{when } i \neq j \text{ or } k \neq l, \tag{9}$$

where the dimensionless parameters α_{ij} are defined as follows:

$$\alpha_{ij} = 1 - \frac{(C^d_{11ij} + C^d_{22ij} + C^d_{33ij})}{3K_s}. \tag{10}$$

For an isotropic material ($C_{1111} = C_{2222} = C_{3333} = K + 4\mu/3$ and $C_{1122} = C_{1133} = C_{2233} = K - 2\mu/3$), equation (8), along with $\mu_u = \mu_d = \mu$ (shear does not create compression in isotropic media), directly reduces to

$$K_u = K_d + \frac{K_s(1 - K_d/K_s)^2}{1 - K_d/K_s - \phi(1 - K_s/K_f)}, \tag{11}$$

which a bit of algebra shows is equivalent to equations (6) and (7) combined.

When calculating anisotropic seismic velocities at seismic frequencies in saturated anisotropic porous material, equations (8) and (9) for C^u_{ijkl} can be used along with models for how C^d_{ijkl} vary with effective stress and crack density as given in the analysis that follows.

3 MODELS FOR HOW THE DRAINED MODULI CHANGE WITH STRESS

In choosing an analytical model for how the drained moduli of rocks change with stress, one is guided not only by the ability of the model to fit laboratory data but by the physical basis of the model, i.e., enough physics must go into the model that it can be predictive and not just purely empirical. Further, since the ultimate goal is to perform the inverse problem and obtain material parameters from time-varying geophysical signals, the number of free parameters that are adjusted to fit laboratory should be kept to a bare minimum, and any such fit parameters should have a clear physical definition so that they can, in principle, be independently measured. Like most researchers before us, to explain the measured stress dependence, we find it necessary to work with a model that has a crack population embedded into a background porous host material, which necessarily adds at least two additional parameters (crack density and crack aspect ratio) to the analysis along with assumptions about the crack orientations. Further, to achieve efficient numerical forward modelling of coupled flow and deformation problems, another objective is to obtain explicit analytical models for how the evolving rock properties depend on stress (as opposed to implicit models or other models that require numerical computation other than function evaluation).

As stated in Section 1, the level of stress and pore-pressure change during industrial applications is likely never more than 10 MPa. We will expand this to consider effective stress

changes over the range of 0–30 MPa. When the isotropic effective pressure (confining pressure minus fluid pressure) exceeds roughly 30 MPa in sandstones, stress concentration at the grain contacts cause some grains to begin to shatter (e.g., Fortin *et al.* 2009), which causes a local collapse in porosity. This is an effect we are not allowing for in this paper. In more crystalline rock, such as granite, purely isotropic stress changes do not result in grain damage until a much larger threshold (hundreds of MPa) is exceeded (e.g., Paterson and Wong 2005).

One class of porous materials that have drained moduli that vary considerably over 0–30 MPa are unconsolidated materials (uncemented grain packs). The reader is referred to Pride (2005) or Pride and Berryman (2009) for analytical models capable of explaining laboratory measurements on grain packs.

3.1 Changes of drained moduli due to changes in porosity

One conceivable approach to modelling how the drained elastic moduli K_d and μ change with applied stress is to focus on how the porosity is changing with stress and to include such porosity variation within any favorite effective medium theory for the drained framework of grains. However, it will be shown here that this approach by itself is not able to explain the pressure dependence of elastic moduli measured on rocks.

By combining the laws of isotropic poroelasticity as given above with the Gassmann relations (6) and (7), Pride (2005) derives the following relation for how porosity changes with stress:

$$d\phi = -\left[\frac{(1-\phi)}{K_d} - \frac{1}{K_s}\right] dP_e, \tag{12}$$

where $P_e = P_c - P$ is the effective pressure. Equation (12) tells us that porosity will only change appreciably if dP_e is on the order of K_d. Since we are not considering effective pressure changes larger than, e.g., $P_e \approx 30$ MPa, this means that porosity change will only be important in materials with a very small drained modulus K_d on the order of 0.1 GPa or smaller. Even weak sandstones tend to be much stiffer than this with drained elastic moduli always larger than 1 GPa and more typically on the order of 10 GPa (see Table 2 in this paper). From this alone, we can conclude that modeling the stress dependence of the elastic moduli by allowing for porosity to change in an effective medium theory will not be able to explain the rather large (e.g., 20%) changes in the elastic moduli of consolidated sandstones that is measured in the laboratory over the range $0 < P_e < 30$ MPa (e.g., Han, Nur and Morgan 1986).

We can make this conclusion even more explicit if we write down an effective medium theory for how K_d (and μ) depend on porosity. One convenient form is (e.g., Pride 2005)

$$K_d = \frac{K_s(1-\phi)}{1 + s_v\phi}, \tag{13}$$

where s_v is a dimensionless time-independent "softness" parameter and K_s is the solid mineral's bulk modulus. The shear modulus has a similar expression with different parameters s_s, μ_s in place of s_v, K_s. One can think of this explicit form as the simplest Padé approximant that ties the low-porosity limit ($K_d \to K_s$) to the high-porosity limit ($K_d \to 0$) and that, through the parameter $s_v > 1$, lies within the Hashin–Shtrickman bounds. Further, when the drained rock consists of a single (isotropic) solid mineral having empty same-shaped ellipsoidal pores randomly embedded into it, the Mori and Tanaka (1973) mean-stress approximation predicts effective moduli of exactly the form (13) with s_v having complicated dependence on the aspect ratio of the embedded ellipses and on the Poisson's ratio of the host mineral. When s_v is modelled according to the Mori and Tanaka theory, Benveniste (1987) has shown that equation (13) lies within the Hashin–Shtrickman bounds (see also Berryman and Berge 1996).

Substituting equation (13) into the law for porosity change gives

$$d\phi = -\frac{s_v\phi}{K_s} dP_e, \tag{14}$$

which upon integration yields

$$\phi(\boldsymbol{\tau}, P) = \phi(0)\mathrm{e}^{-s_v P_e/K_s}. \tag{15}$$

Therefore, the porosity of a rock will only change appreciably if P_e approaches K_s/s_v in amplitude. For a consolidated sandstone, as stated above, K_d might typically be 10 GPa, $\phi = 0.2$, and $K_s = 40$ GPa (quartz), which means that s_v needs to be on the order of 10. As such, equation (15) requires P_e approaching 10^3 MPa for there to be a significant change to the porosity through poroelastic strain. In a sandstone, the grains would be shattering, and the porosity irreversibly collapsing at such high effective pressure. As such, additional considerations, namely the inclusion of a crack population, will be needed in order to explain how the drained elastic moduli depend on stress.

3.2 Cracked rocks

In order to have a model that is consistent with laboratory measurements of how the drained moduli vary with stress, the model we adopt here is one based on there being cracks present in a porous host. The crack porosity is in addition to the porosity between the detrital grains of the host material (sometimes called "equant porosity") that was the only source of porosity before the cracks arrived. New cracks arriving will not be modelled here; only how an already existing crack population influences the elastic properties of a consolidated porous rock. Although the crack porosity is tiny compared with the host porosity for most sedimentary rocks, each crack is far more compliant than an equant pore of the host, and it is the cracks that largely control the stress dependence of the elastic moduli.

There are many possible models available for how cracks influence the elastic properties (e.g., Berryman (2016) provides a review). We will use the approach of Sayers and Kachanov (1995) that is based on the linear-slip crack model describing the normal and tangential displacement discontinuity across crack faces due to tractions imposed on cracks having normal **n**. The linear-slip laws can be written compactly in vector form as

$$[\mathbf{u}] = \mathbf{B} \cdot \boldsymbol{\tau}_e \cdot \mathbf{n}, \tag{16}$$

where $[\mathbf{u}]$ is the displacement discontinuity between the crack faces, $\boldsymbol{\tau}_e$ is the effective stress tensor acting on the crack defined as $\boldsymbol{\tau}_e = \boldsymbol{\tau} + P\mathbf{I}$ (note that the principal components of the stress tensor $\boldsymbol{\tau}$ sum to be positive in tension, whereas the fluid pressure P is positive in compression), and the crack compliance tensor is

$$\mathbf{B} = B_n \mathbf{nn} + B_t(\mathbf{I} - \mathbf{nn}). \tag{17}$$

The key stress dependence of a rock's elastic modulus is contained in how B_n (normal crack compliance) and B_t (tangential crack compliance) vary with stress, which we consider first.

3.2.1 *Exponential stress dependence of B_n and B_t*

For penny-shaped cracks of radius a embedded in a host material having drained elastic moduli of K_{do} and μ_o, the crack compliances prior to stress being applied are finite and given by (e.g., Sayers and Kachanov 1995)

$$\frac{\pi B_n(0)}{a} = \frac{4}{3}\frac{(3K_{do} + 4\mu_o)}{\mu_o(3K_{do} + \mu_o)} = \frac{16}{3}\frac{(1-\nu_o^2)}{E_o}, \tag{18}$$

$$\frac{\pi B_t(0)}{a} = \frac{16}{9}\frac{(3K_{do} + 4\mu_o)}{(3K_{do} + 2\mu_o)} = \frac{32}{3}\frac{(1-\nu_o^2)}{E_o(2-\nu_o)}. \tag{19}$$

A model for how K_{do} and μ_o depend on the host porosity ϕ_o can be proposed if desired. In the second form of each expression, we have replaced the drained bulk and shear modulus of the host material with the drained Young's modulus E_o and Poisson's ratio ν_o, where $K_{do} = E_o/[3(1-2\nu_o)]$ and $\mu_o = E_o/[2(1+\nu_o)]$.

Once compressive stress is added, the cracks will begin to close and strengthen causing the crack compliances to decrease from the above values and the rock to stiffen. If $\boldsymbol{\tau}_e$ is not purely isotropic so that $\boldsymbol{\tau}_e = -P_e\mathbf{I} + \boldsymbol{\tau}_e^D$ where $\boldsymbol{\tau}_e^D$ is the deviatoric portion, then even if the cracks are isotropically oriented in space at zero stress, once $\boldsymbol{\tau}_e^D$ is applied to a sample, cracks in different orientations will strengthen differently resulting in the rock sample becoming elastically anisotropic. Although in the comparison to data, we will, for convenience, take $\tau_n^e = -P_e$ (normal component of the effective traction) and $\tau_t^e = 0$ (transverse component of the effective traction) in modelling the stress interaction with a crack population so that a sample remains isotropic with increasing stress; in the development that follows, we will retain the general definitions of equation (16) that allows for deviatoric stress and thus allows for emergent anisotropy.

In order to obtain the stress dependence of the crack compliances, we focus on the fracture aperture w, which is the effective width of the gap present between the crack faces. A change in the crack aperture dw brought on by a change in the normal effective traction component $d\tau_n^e = \mathbf{n} \cdot d\boldsymbol{\tau}_e \cdot \mathbf{n}$ is assumed governed by a Hooke's law:

$$d\tau_n^e = \sigma_n \frac{dw}{w}, \tag{20}$$

where the effective elastic modulus of the crack σ_n will be determined shortly. We assume linear elasticity so that the modulus σ_n is independent of stress. Integrating this equation gives an expression for how the crack aperture varies with stress:

$$w(\tau_n^e) = w(0)\mathrm{e}^{\tau_n^e/\sigma_n}, \tag{21}$$

where $w(0)$ is the aperture at zero stress. Then, by definition of the normal crack compliance, we have

$$B_n(\tau_n^e) = \frac{dw(\tau_n^e)}{d\tau_n^e} = \frac{w(0)}{\sigma_n}\,\mathrm{e}^{\tau_n^e/\sigma_n}. \tag{22}$$

By requiring $B_n(0)$ to be given by equation (18), the crack modulus is identified as

$$\sigma_n = \frac{\pi w(0)}{a}\frac{3E_o}{16(1-\nu_o^2)}. \tag{23}$$

To make explicit the dependence on the aspect ratio

$$\epsilon = \frac{w(0)}{2a}, \tag{24}$$

we write the crack-compliance stress dependence as

$$B_n(\tau_n^e) = B_n(0)\ \mathrm{e}^{\tau_n^e/(\epsilon C_n)}, \tag{25}$$

where the stiffness property of the host phase C_n is defined from equation (23) as

$$C_n = \frac{3\pi E_o}{8\left(1-\nu_o^2\right)}. \tag{26}$$

The modulus $\sigma_n = \epsilon C_n$ can be interpreted as setting the stress scale required for closing the cracks.

To obtain how B_t varies with stress, let dh represent a tangential displacement of one crack face relative to the other brought on by the application of the shear-stress increment $d\tau_t^e = \sqrt{|\mathbf{n}\cdot d\boldsymbol{\tau}_e|^2 - (\mathbf{n}\cdot d\boldsymbol{\tau}_e\cdot\mathbf{n})^2}$. A Hooke's law is then given as follows:

$$d\tau_t^e = \sigma_t \frac{dh}{w}, \tag{27}$$

which directly gives from the definition of the tangential crack compliance:

$$B_t(\tau_n^e) = \frac{dh}{d\tau_t^e} = \frac{w(0)}{\sigma_t}\mathrm{e}^{\tau_n^e/(\epsilon C_n)}. \tag{28}$$

We can then use this expression at $\tau_n^e = 0$ to identify the elastic shear modulus of the crack σ_t from equation (19), which gives

$$B_t(\tau_n^e) = B_t(0)\mathrm{e}^{\tau_n^e/(\epsilon C_n)}. \tag{29}$$

We will show later that this stress dependence can explain how seismic velocities in sandstones vary with stress. Schoenberg (2002) assumes the above exponential model for B_n and B_t without discussion or derivation as have Zhang *et al.* (2009) and Sayers and den Boer (2011).

We have also modelled the crack compliances B_n and B_t using the "bed-of-nails" model of Gangi (1978) that allows for a range of asperity heights in the gap of the crack; with increasing applied stress, more asperities come into contact and the crack stiffens. Due to the specific assumptions that must be made to obtain analytical final results, the Gangi bed-of-nails model does not do as good a job matching data on sandstones (e.g., Han *et al.* 1986) and involves more unconstrained parameters compared with the simple exponential model that only involves the aspect ratio of a crack and the elastic moduli of the host material. As such, we have elected to use the above exponential-stress model for B_n and B_t in this work.

3.2.2 *The elastic moduli of a porous rock hosting a crack population*

We follow the approach of Sayers and Kachanov (1995), which is equivalent to Schoenberg and Sayers (1995) and Schoenberg (2002), in their modelling of how a population of cracks influences the elastic compliances (not stiffnesses) S_{ijkl} of a dry porous rock. Since the derivation of this effective medium theory is straightforward and because we perform the averaging over the crack population differently than Sayers and Kachanov (1995), we present a self-contained development.

The average strain tensor e_{ij} in a sample Ω of volume V is defined:

$$e_{ij} = \frac{1}{2V}\int_\Omega (\partial_i u_j + \partial_j u_i)\, dV, \tag{30}$$

where u_i are the displacements throughout the sample and ∂_i is the gradient operator. Lets decompose the sample into host (o) and crack (2) regions $\Omega = \Omega_o + \Omega_2$ with $V = V_o + V_2$. We then write

$$e_{ij} = \frac{1}{2V}\left[\int_{\Omega_o}(\partial_i u_j + \partial_j u_i)\, dV + \int_{\partial\Omega_2}(n_i u_j + n_j u_i)\, dS\right], \tag{31}$$

where $\partial\Omega_2$ is the surface surrounding all the cracks. If we assume the cracks are thin and symmetric about their minor axis (e.g., penny shaped), a plane surface S_c can be made to pass down the centre of each crack with a normal $\mathbf{n}$ that is in the direction of the minor axis. We can then write

$$e_{ij} = (1-\phi_2)e_{ij}^o + \frac{1}{2V}\sum_c \int_{S_c}(n_i[u_j] + n_j[u_i])\, dS, \tag{32}$$

where e_{ij}^o is the average strain throughout the host, ϕ_2 the porosity of all the cracks, and $[u_i]$ the jump discontinuity in displacement from one face of a penny-shaped crack to the other.

Making a mean-field approximation that a uniform stress tensor τ_{ij} acts throughout the host phase and on each crack, we can write $e_{ij}^o = S_{ijkl}^o\tau_{kl}$, where S_{ijkl}^o is the effective compliance tensor of the host and $[u_i] = B_{ik}\tau_{kl}n_l = B_{il}\tau_{lk}n_k = (B_{ik}n_l + B_{il}n_k)\tau_{kl}/2$ from equation (16). If we further introduce the crack-compliance tensor of equation (17) and assume that such discontinuity is uniform across each crack of surface area S_c, we have

$$e_{ij} = (1-\phi_2)S_{ijkl}^o\tau_{kl} + \Delta e_{ij}, \tag{33}$$

where Δe_{ij} is the strain contribution coming from the cracks and given by

$$\Delta e_{ij} = \frac{1}{V}\sum_c S_c \Big[(B_n - B_t) n_i n_j n_k n_l + \frac{B_t}{4}\left(\delta_{ik}n_l n_j + \delta_{jk}n_l n_i + \delta_{il}n_k n_j + \delta_{jl}n_i n_k\right)\Big]\tau_{kl}. \tag{34}$$

The effective compliance tensor of the cracked sample is then written:

$$S_{ijkl} = (1-\phi_2)S^o_{ijkl} + \Delta S_{ijkl}, \tag{35}$$

with the crack perturbations ΔS_{ijkl} given by

$$\Delta S_{ijkl} = \frac{N}{V}\left\{ \frac{1}{N}\sum_c S_c \Big[(B_n - B_t) n_i n_j n_k n_l + \frac{B_t}{4}\left(\delta_{ik}n_l n_j + \delta_{jk}n_l n_i + \delta_{il}n_k n_j + \delta_{jl}n_i n_k\right)\Big]\right\}. \tag{36}$$

Here, N is the total number of cracks in the system, and the curly brackets contain an average over the crack population.

The above formalism due to Sayers and Kachanov (1995) allows one or more larger deterministic fractures to be present in each sample Ω or many smaller randomly oriented cracks or some combination of the two. The central approximation in this theory is using the mean stress to determine the linear-slip discontinuities, and this approximation improves when the cracks have some randomness to their orientations. Assuming penny-shaped cracks for which $S_c = \pi a^2$, the compliances B_n and B_t were shown earlier to depend on the aspect ratio $\epsilon = w(0)/(2a) = b(0)/a$ where $b(0)$ is the minor semi-axis length of the crack when $\tau^e_n = 0$ (c.f., Fig. 1).

Using $p_{\epsilon|a}(\epsilon|a)\,p_a(a)da\,d\epsilon$ to represent the probability that any one crack has a radius within the range $[a, a+da]$ and an aspect ratio within $[\epsilon, \epsilon+d\epsilon]$, we rewrite the average over the cracks to obtain

$$\Delta S_{ijkl} = \frac{N}{V}\beta_t \int\int da\,d\epsilon\; p_{\epsilon|a}(\epsilon|a)p_a(a)a^3 \times \left(\frac{\delta_{ik}g_{jl} + \delta_{jk}g_{il} + \delta_{il}g_{kj} + \delta_{jl}g_{ik}}{2} - \nu_o h_{ijkl}\right), \tag{37}$$

where the compliance β_t is defined from equation (19) as

$$\beta_t = \frac{\pi B_t}{2a} = \frac{16}{3}\frac{(1-\nu_o^2)}{E_o(2-\nu_o)} = \frac{2\pi}{C_n(2-\nu_o)}. \tag{38}$$

The crack orientation tensors (g_{ij} and h_{ijkl}) are obtained as averages over a specified range of crack-normal orientations

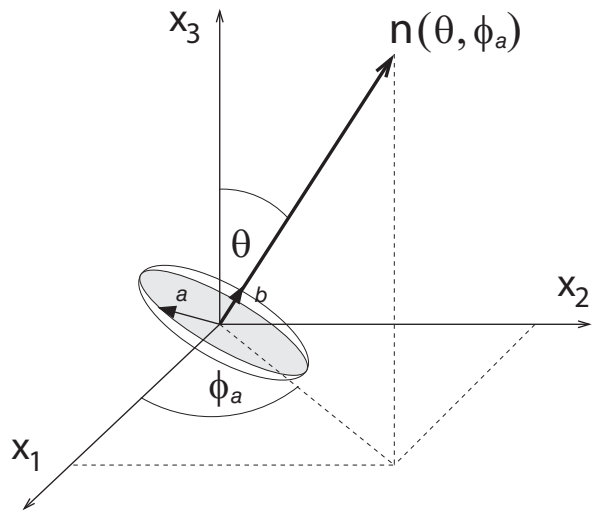

Figure 1 Coordinates used to define the orientation of the crack normal $\mathbf{n}(\theta, \phi_a)$. A crack is modelled here as an oblate spheroid (or penny-shaped crack) having a major radius a and a minor semi-axis length b. The aspect ratio is $\epsilon = b/a$.

$n_i(\theta, \phi_a)$ using solid angles:

$$g_{ij}(a,\epsilon) = \frac{1}{A(a,\epsilon)}\int_{\theta_-(a,\epsilon)}^{\theta_+(a,\epsilon)} \sin\theta\, d\theta \int_{\phi_{a-}(a,\epsilon)}^{\phi_{a+}(a,\epsilon)} d\phi_a \times n_i(\theta,\phi_a)n_j(\theta,\phi_a)\exp\left[\frac{n_p(\theta,\phi_a)n_q(\theta,\phi_a)\tau^e_{pq}}{\epsilon C_n}\right], \tag{39}$$

$$h_{ijkl}(a,\epsilon) = \frac{1}{A(a,\epsilon)}\int_{\theta_-(a,\epsilon)}^{\theta_+(a,\epsilon)} \sin\theta\, d\theta \int_{\phi_{a-}(a,\epsilon)}^{\phi_{a+}(a,\epsilon)} d\phi_a \times n_i(\theta,\phi_a)n_j(\theta,\phi_a)n_k(\theta,\phi_a)n_l(\theta,\phi_a) \times \exp\left[\frac{n_p(\theta,\phi_a)n_q(\theta,\phi_a)\tau^e_{pq}}{\epsilon C_n}\right]. \tag{40}$$

The angles θ and ϕ_a that define the crack orientations are given in relation to the coordinate directions $\hat{\mathbf{x}}_i$ in Fig. 1. The total solid angle A being integrated over in the average depends on the range of angles $[\theta_-, \theta_+]$ and $[\phi_{a-}, \phi_{a+}]$, over which each crack type (a, ϵ) has random orientations and is given by

$$A = \int_{\theta_-}^{\theta_+}\sin\theta\, d\theta\int_{\phi_{a-}}^{\phi_{a+}} d\phi_a = \left(\phi_{a+} - \phi_{a-}\right)\left(\cos\theta_- - \cos\theta_+\right). \tag{41}$$

As shown in Fig. 1, the crack normal $\mathbf{n}$ is given by

$$\mathbf{n}(\theta,\phi_a) = \sin\theta\,(\cos\phi_a\hat{\mathbf{x}}_1 + \sin\phi_a\hat{\mathbf{x}}_2) + \cos\theta\hat{\mathbf{x}}_3. \tag{42}$$

By choosing the ranges $[\theta_-, \theta_+]$ and $[\phi_{a-}, \phi_{a+}]$ for each type of crack (a, ϵ), various types of anisotropy can be allowed

for. Even if the cracks are isotropically oriented over all possible angles, so long as $\boldsymbol{\tau}_e$ has a deviatoric component, there will emerge a stress-induced anisotropy as deviatoric stress increases from zero.

In the case of isotropic stress $\boldsymbol{\tau}_e = -P_e \mathbf{I}$ and isotropic crack orientations $\theta_- = 0$, $\theta_+ = \pi$, $\phi_{a-} = 0$, $\phi_{a+} = 2\pi$, and $A = 4\pi$, the integrals (39) and (40) can be performed analytically to give

$$g_{ij} = \frac{\delta_{ij}}{3} \mathrm{e}^{-P_e/(C_n \epsilon)}, \tag{43}$$

and

$$h_{ijkl} = \frac{1}{15} \left(\delta_{ij}\delta_{kl} + \delta_{ik}\delta_{jl} + \delta_{il}\delta_{jk} \right) \mathrm{e}^{-P_e/(C_n \epsilon)}. \tag{44}$$

These are indeed seen to be isotropic second-order and fourth-order tensors.

In all that follows, we assume that the probability of observing a crack to have an aspect ratio ϵ is statistically independent from the crack's radius a so that $p_{\epsilon|a}(\epsilon|a) = p_\epsilon(\epsilon)$. We can then perform the integral over a to define a crack-density parameter ρ_c as

$$\rho_c = \frac{N}{V} \int da \; p_a(a) a^3 = \frac{N}{V} \langle a^3 \rangle. \tag{45}$$

In the case of isotropic stress $\tau^e_{pq} = -P_e \delta_{pq}$ and isotropic crack orientations, the perturbation of the compliances is

$$\Delta S_{ijkl} = \frac{\rho_c \beta_t}{15} \left[(5 - \nu_o) \left(\delta_{ik}\delta_{jl} + \delta_{jk}\delta_{il} \right) - \nu_o \delta_{ij}\delta_{kl} \right] f(P_e), \tag{46}$$

where the effective stress function is:

$$f(P_e) = \int d\epsilon \; p_\epsilon(\epsilon) \mathrm{e}^{-P_e/(C_n \epsilon)}. \tag{47}$$

When the host material is isotropic, we also have

$$S^o_{ijkl} = \frac{(1 + \nu_o)}{2E_o} \left(\delta_{ik}\delta_{jl} + \delta_{jk}\delta_{il} \right) - \frac{\nu_o}{E_o} \delta_{ij}\delta_{kl}, \tag{48}$$

so that the non-zero compliances of the fractured rock in the fully isotropic case are given by

$$S_{1111} = S_{2222} = S_{3333} = \frac{1}{E_o} + \rho_c \beta_t \left(\frac{2}{3} - \frac{\nu_o}{5} \right) f(P_e), \tag{49}$$

$$S_{1122} = S_{1133} = S_{2233} = -\frac{\nu_o}{E_o} - \rho_c \beta_t \frac{\nu_o}{15} f(P_e), \tag{50}$$

$$S_{1212} = S_{1313} = S_{2323} = \frac{(1 + \nu_o)}{E_o} + \rho_c \beta_t \left(\frac{1}{3} - \frac{\nu_o}{15} \right) f(P_e). \tag{51}$$

We see that $S_{1212} = (S_{1111} - S_{1122})/2$, which is a general requirement of any isotropic elastic material and is a consistency check. Equations (49)–(51) and (47) determine how the elastic constants depend on crack density ρ_c and effective stress P_e in an isotropic cracked porous material.

Finally, by inverting the isotropic compliance tensor, we obtain the bulk and shear moduli of the isotropic cracked rock as

$$K_d(P_e) = \frac{1}{3(S_{1111} + 2S_{1122})}, \tag{52}$$

$$\mu(P_e) = \frac{1}{2(S_{1111} - S_{1122})} = \frac{1}{4S_{1212}}. \tag{53}$$

At high effective pressure, where cracks are mainly closed, these moduli are set by the moduli K_{do} (or E_o) and ν_o of the non-cracked host rock. At low effective pressure, where the cracks are open, the associated decrease in the moduli is controlled by the crack density ρ_c, which is independent of P_e. The transition of the moduli from low to high pressures is set by the functional nature of the aspect-ratio probability distribution p_ϵ and the range of aspect ratios present as equation (47) for $f(P_e)$ makes clear.

In cases of a general stress tensor with deviatoric stress present and where the cracks are grouped into subsets s within which all cracks in the subset have the same orientation θ_s and ϕ_{as} and a crack density $\rho^{(s)}_c = N_s \langle a^3 \rangle / V$ such that $\rho_c = \sum_{s=1}^{M} \rho^{(s)}_c$ for all M subsets, we obtain the anisotropic form of the above

$$S_{ijkl} = S^o_{ijkl} + \beta_t \sum_{s=1}^{M} \rho^{(s)}_c \left(\frac{\delta_{ik} g^{(s)}_{jl} + \delta_{jk} g^{(s)}_{il} + \delta_{jk} g^{(s)}_{il} + \delta_{jl} g^{(s)}_{ik}}{2} - \nu_o h^{(s)}_{ijkl} \right) f_s(\tau^e_{pq}). \tag{54}$$

The crack normals of subset s are defined

$$n^{(s)}_1 = \sin\theta_s \cos\phi_{as}, \tag{55}$$

$$n^{(s)}_2 = \sin\theta_s \sin\phi_{as}, \tag{56}$$

$$n^{(s)}_3 = \cos\theta_s, \tag{57}$$

where θ_s and ϕ_{as} are the orientation angles for all cracks in this subset of all cracks. The crack orientation tensors for subset s are then simply read off from equations (39) and (40) as

$$g^{(s)}_{ij} = n^{(s)}_i n^{(s)}_j \exp\left(\frac{n^{(s)}_p n^{(s)}_q \tau^e_{pq}}{C_n \epsilon} \right), \tag{58}$$

and

$$h^{(s)}_{ijkl} = n^{(s)}_i n^{(s)}_j n^{(s)}_k n^{(s)}_l \exp\left(\frac{n^{(s)}_p n^{(s)}_q \tau^e_{pq}}{C_n \epsilon} \right). \tag{59}$$

These expressions are independent of each crack's radius a. All stress dependence of each subset is defined by the function

$$f_s\left(\tau^e_{pq}\right) = \int d\epsilon\; p_\epsilon(\epsilon) \exp\left(\frac{n^{(s)}_p n^{(s)}_q \tau^e_{pq}}{C_n \epsilon}\right), \tag{60}$$

with crack normals again given by equations (55) – (57). These expressions work even if $M = 1$ (the entire crack population having one orientation).

3.3 Porosity change when cracks are present

We can translate the crack density ρ_c into a crack porosity ϕ_2 and thus obtain an expression for how the porosity of the entire rock is changing with stress. Assuming penny-shaped cracks with each crack having volume $4\pi a^2 b/3$ and with the total volume of all cracks being V_2, one obtains

$$\phi_2(P_e) = \frac{V_2}{V} = \frac{4\pi}{3}\langle\epsilon(P_e)\rangle\rho_c, \tag{61}$$

where the average aspect ratio as a function of P_e is

$$\langle\epsilon(P_e)\rangle = \int p_\epsilon(\epsilon)\,\epsilon\, \mathrm{e}^{-P_e/(C_n\epsilon)}\, d\epsilon. \tag{62}$$

This expression for ϕ_2 formally assumes that the cracks do not overlap. For overlapping cracks of a single-aspect ratio, one replaces ϕ_2 on the left-hand side of equation (61) with $-\ln(1-\phi_2)$ (e.g., Garboczi *et al.* 1991) which reduces to ϕ_2 in the common case where $\phi_2 \ll 1$, i.e., even if cracks are overlapping, the volume of their intersection is negligible when the aspect ratios are small.

The total porosity of the rock is then given as follows:

$$\phi(P_e) = \frac{(V - V_2)\phi_o + V_2}{V} = \phi_o + (1-\phi_o)\rho_c \frac{4\pi}{3}\langle\epsilon(P_e)\rangle, \tag{63}$$

where we are using that the host porosity ϕ_o is the fraction of the non-cracked volume $V - V_2$ that is occupied by pores. Although the crack porosity V_2/V is varying strongly with P_e, there simply may not be much crack porosity contributing to the total porosity, especially in sandstones.

Taking a derivative of equation (63) gives

$$d\phi = \left(1 - \rho_c \frac{4\pi}{3}\langle\epsilon(P_e)\rangle\right) d\phi_o - (1-\phi_o)\rho_c \frac{4\pi}{3C_n} f(P_e)\, dP_e. \tag{64}$$

In this expression, $f(P_e)$ is given by equation (47) and $\langle\epsilon(P_e)\rangle$ by equation (62). Earlier, we showed that when no cracks are present, the change $d\phi_o$ of the background host phase is negligible. However, with cracks being present, the change of the background host porosity can be more important.

The earlier expression (12) for the total change in connected porosity, which is an exact result of poroelasticity for monomineral Gassmann materials, is still valid once cracks are present; however, we must use the expression for $K_d(P_e)$ given by equation (52) that allows for the crack population, i.e.,

$$d\phi = -\left(\frac{(1-\phi)}{K_d(P_e)} - \frac{1}{K_s}\right) dP_e. \tag{65}$$

This expression is the one we will use to compare to data on how porosity varies with P_e.

To know how the background host porosity ϕ_o is changing with P_e, equations (64) and (65) are equated. For sandstones or other porous rocks with porosity on the order of a few percent or more, it is justified to take $\phi \approx \phi_o$ in equation (65) when doing so. The result is

$$\frac{d\phi_o}{dP_e} = \frac{(1-\phi_o)\rho_c f(P_e) 4\pi/(3C_n) - (1-\phi_o)/K_d(P_e) + 1/K_s}{1 - \rho_c\langle\epsilon(P_e)\rangle 4\pi/3}. \tag{66}$$

This non-linear differential equation determines $\phi_o(P_e)$ starting from an initial condition. With $\phi_o(P_e)$ known, the drained moduli of the background host will vary with P_e according to equation (13).

We earlier showed in Section 3.1 that the porosity of the background host material does not vary significantly with P_e (at least over the 0–30 MPa range of interest) in the absence of a crack population. However, with a crack population, equation (66) allows $\phi_o(P_e)$ to vary more significantly with effective stress, and accordingly, $K_{do}(P_e)$ and $\mu_o(P_e)$ can be considered to vary using a favorite effective medium theory such as given earlier by equation (13).

4 MODELS FOR HOW PERMEABILITY AND FORMATION FACTOR CHANGE WITH STRESS

Here, we allow for how the porespace properties of permeability k and formation factor F are varying with stress as influenced by the crack population. As discussed in the later Section 5.2, the formation factor is the key geometric property of the porespace controlling the overall electrical conductivity of the rock. In what follows, a subscript o always refers to the background host phase.

4.1 Permeability of the host material as a function of stress

To allow for how the permeability of the host phase is evolving with stress, we assume the permeability of the host obeys a law of the form $k_o = c\,\ell_o^2/F_o$ (e.g., Johnson, Koplik, and Schwartz 1986; Thompson, Katz, and Krohn 1987), where F_o is the formation factor of the host, ℓ_o is an appropriate pore size, and c is a time-independent constant that depends on the precise definition of ℓ_o and will not be of importance. Taking the derivative one has

$$\frac{dk_o}{k_o} = 2\frac{d\ell_o}{\ell_o} - \frac{dF_o}{F_o}. \tag{67}$$

The host's pore volume goes as $V_{\phi o} = N_\phi \ell_o^3$ where N_ϕ is a time-independent constant; this form is appropriate for the equant pores of the host phase. Taking the derivative gives $d\ell_o/\ell_o = dV_{\phi_o}/(3V_\phi)$, where from the definition $\phi_o = V_{\phi o}/V_o$ gives $dV_{\phi o} = V_o d\phi_o - \phi_o dV_o$ with $d\phi_o$ given by equation (12) and $dV_o/V_o = -(dP_c - \alpha_o dP)/K_{do}$ by one of the isotropic poroelasticity laws. If we further assume the formation factor of the host to be given by Archie's (1942) law $F_o = \phi_o^{-m}$, where m is another time-independent constant, the earlier poroelasticity laws of Section 3.1 give the permeability evolution equation of the host as follows (e.g., Pride 2005):

$$\frac{dk_o}{k_o} = -C_k(dP_c - \alpha_k dP), \tag{68}$$

where the permeability compliance of the host is defined as

$$C_k = \frac{2\alpha_o/3 + m(\alpha_o - \phi_o)}{\phi_o K_{do}}, \tag{69}$$

and where the permeability effective-stress coefficient of the host is

$$\alpha_k = \frac{\phi_o\alpha_o m - (2/3+m)(\alpha_o/B_o - \phi_o)}{\phi_o m - (2/3+m)\alpha_o}. \tag{70}$$

In these coefficients, $\alpha_o = 1 - K_{do}/K_s$, B_o, and K_{do} are the poroelastic moduli of the host phase. Both C_k and α_k depend on P_e through $\phi_o(P_e)$ and $K_{do}(P_e)$ [e.g., equation (13)]. The permeability has a different effective-stress coefficient (α_k) compared with that of the porosity and drained moduli of the host (unity) because, although the porosity and the drained moduli are scale invariant (their values do not change if the porous host is uniformly expanded or contracted in size), the permeability is not scale invariant.

If in a first approximation the porosity and elastic moduli of the host are assumed to vary negligibly with stress over the stress range 0–30 MPa, equation (68) can then be integrated analytically to obtain the explicit form as follows:

$$k_o(\boldsymbol{\tau}, P) = k_o(0)\mathrm{e}^{-C_k(P_c - \alpha_k P)}. \tag{71}$$

However, in the comparison to laboratory data, we find in Section 5 that it is somewhat better to allow for the coefficients C_k and α_k to vary with stress and to determine the associated change of host permeability at each stress increment using equation (68).

In what follows, we assume that the formation factor of the host material follows Archie's law $F_o = \phi_o^{-m}$ with ϕ_o determined from equation (66).

4.2 The permeability and formation factor of a porous rock hosting a crack population

To treat how a crack population influences the permeability, Oda (1985) adopts a mean-field approach in which a uniform pressure gradient is driving flow both through the background porous-host phase and through the crack population. The Oda (1985) approach is directly analogous to the Sayers and Kachanov (1995) treatment of how the average stress creates strain in both the host and crack phases. Here, we use the Oda (1985) approach to obtain the effective permeability of a cracked rock as well as the formation factor (a problem not considered by Oda, (1985)) and do so using the same formalism (e.g., the definition of the crack density) as used in the elastic moduli modeling, which is distinct from Oda's (1985) presentation.

To obtain an expression for the effective permeability, focus is placed on the mean Darcy flux $\mathbf{q}$ through a sample that is again divided into a host phase Ω_o and crack phase Ω_2 (with $V = V_o + V_2$). We have

$$\mathbf{q} = \frac{1}{V}\left[\int_{\Omega_o} \mathbf{q}_o\, dV + \int_{\Omega_2} \mathbf{v}_f\, dV\right] \tag{72}$$

$$= \frac{1}{V}\left[V_o\bar{\mathbf{q}}_o + \frac{4\pi}{3}\sum_c \bar{\mathbf{v}}_{fc}\, b_c\, a_c^2\right] \tag{73}$$

$$= (1-\phi_2)\bar{\mathbf{q}}_o + \frac{4\pi}{3}\frac{N}{V}\left\{\frac{1}{N}\sum_c \bar{\mathbf{v}}_{fc}\, b_c\, a_c^2\right\}. \tag{74}$$

Here, $\mathbf{q}_o$ is the local Darcy flux in the host phase and $\bar{\mathbf{q}}_o$ is the average Darcy flux in the host phase. Similarly, $\mathbf{v}_f$ is the local fluid velocity in the cracks, and $\bar{\mathbf{v}}_{fc}$ is the average fluid velocity in a particular crack c. The mean-field approximation assumes that $-\nabla P$ is the mean force density driving flow throughout the entire sample so that $\bar{\mathbf{q}}_o = -\mathbf{k}_o \cdot \nabla P/\eta$, where η is the fluid viscosity and $\mathbf{k}_o$ is the permeability tensor of the host. After averaging the Poisseuile flow in a crack having minor axis b_c, we obtain

$$\bar{\mathbf{v}}_{fc} = -\frac{b_c^2}{\nu_k}(\mathbf{I} - \mathbf{nn}) \cdot \frac{\nabla P}{\eta}, \tag{75}$$

where the prefactor ν_k is equal to 3 if the crack is modelled as a planar gap of infinite extent and, as noted by Oda (1985), will be larger than 3 for cracks of finite extent (such as penny-shaped cracks). For the time being, we retain ν_k as a fitting term to be determined, while expecting $\nu_k \geq 3$, but will more thoroughly model ν_k in the percolation model of Section 4.4. In the above, we are following Oda (1985) and Kachanov (1980) in assuming that only the component of the macroscopic pressure gradient that is parallel with the crack contributes to flow in the crack. The cracks are so thin that the fluid flow perpendicular to a crack is controlled entirely by the flow in the host and need not be separately allowed for.

Thus, in the overall effective Darcy law for the sample $q_i = -k_{ij}\partial_j P/\eta$, the effective permeability tensor is given by

$$k_{ij} = (1-\phi_2)k^o_{ij} + \frac{4\pi}{3\nu_k}\frac{N}{V}\left\{\frac{1}{N}\sum_c b_c^3 a_c^2(\delta_{ij} - n_i n_j)\right\}, \tag{76}$$

$$= (1-\phi_2)k^o_{ij} + \frac{4\pi}{3\nu_k}\frac{N}{V}\iint d\epsilon\, da\; p_{\epsilon|a}(\epsilon)p_a(a)\epsilon^3 a^5 c_{ij}(a,\epsilon), \tag{77}$$

where the aspect ratio $\epsilon = b_c(0)/a_c$ is again defined at zero effective stress and the tensor c_{ij} is defined as

$$c_{ij}(a,\epsilon) = \frac{1}{A}\int_{\theta_-}^{\theta^+} d\theta \int_{\phi_{a-}}^{\phi_{a+}} d\phi_a \left[\delta_{ij} - n_i(\theta,\phi_a)n_j(\theta,\phi_a)\right] \times \exp\left(\frac{3n_p(\theta,\phi_a)n_q(\theta,\phi_a)\tau^e_{pq}}{C_n\epsilon}\right). \tag{78}$$

The factor of 3 in the exponential is from the cubic dependence on aperture. The solid angle A being integrated over is given by equation (41) and the crack normal $n_i(\theta,\phi_a)$ by equation (42).

For the special case of all cracks having the same orientation with a normal given by equations (55)–(57), the averaging over the angles can be dispensed with to obtain

$$c_{ij} = \left(\delta_{ij} - n_i n_j\right)\exp\left(\frac{3n_p(\theta,\phi_a)n_q(\theta,\phi_a)\tau^e_{pq}}{C_n\epsilon}\right), \tag{79}$$

which has no dependence on a and an ϵ dependence confined to the exponential.

If we now specialise to the case of isotropy so that $\boldsymbol{\tau}_e = -P_e\mathbf{I}$, $c_{ij} = 2\delta_{ij}/3$ and $k^o_{ij} = k_o\delta_{ij}$ and if the aspect ratios of the cracks are uncorrelated to crack radius, then the effective isotropic permeability k is

$$k = (1-\phi_2)k_o + \frac{8\pi}{9\nu_k}\rho_c\frac{\langle a^5\rangle}{\langle a^3\rangle}\int d\epsilon\; p_\epsilon(\epsilon)\epsilon^3\, \mathrm{e}^{-3P_e/(C_n\epsilon)}. \tag{80}$$

Here, $\rho_c = N\langle a^3\rangle/V$ is the crack density and angle brackets denote averaging using the probability density $p_a(a)$. If we introduce the crack porosity ϕ_2 through the relation $\rho_c = 3\phi_2/(4\pi\langle\epsilon(P_e)\rangle)$ of equation (61) and use the fact that $\phi_2 \ll 1$ in all applications to rocks, we can rewrite equation (80) as

$$k = k_o + \frac{2\phi_2}{3\nu_k}\frac{\langle a^5\rangle}{\langle a^3\rangle}\frac{\langle\epsilon(P_e)^3\rangle}{\langle\epsilon(P_e)\rangle}, \tag{81}$$

where we introduced the notation $\langle\epsilon(P_e)^n\rangle = \int d\epsilon\; p_\epsilon(\epsilon)\epsilon^n \exp[-nP_e/(C_n\epsilon)]$ for any power n.

To obtain the equivalent mean-field approximation for the inverse formation factor tensor $G_{ij} = F^{-1}_{ij}$, we retain the above formalism but replace b_c^2/ν_k with $1/\nu_G$ in the expression for the mean flux through each crack, where $\nu_G = 1$ for cracks modelled as infinite planar gaps and $\nu_G > 1$ for cracks of finite extent. We obtain

$$G_{ij} = F^{-1}_{ij} = (1-\phi_2)G^o_{ij} + \frac{4\pi}{3\nu_G}\frac{N}{V}\left\{\frac{1}{N}\sum_c b_c a_c^2(\delta_{ij} - n_i n_j)\right\}, \tag{82}$$

$$= (1-\phi_2)G^o_{ij} + \frac{4\pi}{3\nu_G}\frac{N}{V}\iint d\epsilon\, da\; p_{\epsilon|a}(\epsilon)p_a(a)\epsilon a^3 d_{ij}(a,\epsilon), \tag{83}$$

where the tensor d_{ij} is defined as

$$d_{ij}(a,\epsilon) = \frac{1}{A}\int_{\theta_-}^{\theta^+} d\theta \int_{\phi_{a-}}^{\phi_{a+}} d\phi_a \left[\delta_{ij} - n_i(\theta,\phi_a)n_j(\theta,\phi_a)\right] \times \exp\left[\frac{n_p(\theta,\phi_a)n_q(\theta,\phi_a)\tau^e_{pq}}{C_n\epsilon}\right]. \tag{84}$$

The difference between d_{ij} and c_{ij} is the factor of 3 in the exponential. The inverse formation factor of the host can be modelled as being isotropic $G^o_{ij} = G_o\delta_{ij}$, where G_o can be modeled using Archie's (1942) law $G_o = \phi_o^m$ or any favorite model. In this case, all electrical anisotropy is due to the crack population alone.

If we specialise to the case of isotropic stress and crack orientations, we take $\boldsymbol{\tau}_e = -P_e\mathbf{I}$ to obtain

$$G = \frac{1}{F} = (1-\phi_2)G_o + \frac{8\pi}{9\nu_G}\rho_c\int d\epsilon\; p_\epsilon(\epsilon)\epsilon\, \mathrm{e}^{-P_e/(C_n\epsilon)}. \tag{85}$$

This will be the model of inverse formation factor to be compared with data. From equation (61), we again have $\rho_c = 3\phi_2/(4\pi\langle\epsilon(P_e)\rangle)$, which along with the fact that $\phi_2 \ll 1$, allows equation (85) to be rewritten in the compact form:

$$G = G_o + \frac{2\phi_2}{3\nu_G}. \tag{86}$$

In the following section, we will see that when the background host phase is sufficiently conductive and when the aspect ratio

of the cracks is sufficiently small, then $\nu_G = 1$ is an excellent approximation. Under these same conditions, we will also see that taking $\nu_k = 3$ is equivalently good in the permeability model.

Similar to the model for the overall rock compliance, the above non-interacting-crack mean-field model has both permeability and inverse formation factor linear in the crack density ρ_c. This is likely adequate for most applications in which the host is both permeable and conductive. However, when the host is not permeable or conductive, this model clearly runs into problems for populations at low crack densities where the cracks do not percolate across the sample and yet the model predicts a finite permeability or conductivity for the rock sample. A percolation extension of the above model is therefore explored next.

4.3 Percolation model for electrical conduction

We develop an alternative model that says once the randomly positioned crack population reaches a critical crack density $\tilde{\rho}_c$, the cracks will overlap with one another sufficiently to allow a continuous transport path through the crack phase. It will be convenient to first develop the model in terms of the crack porosity ϕ_2 and then convert the problem back to crack density at the end if desired. The central limitation of the percolation model presented here is that what is known at present about percolation of penny-shaped cracks involves crack populations of a single aspect ratio and crack radius [$p_\epsilon = \delta(\epsilon - \epsilon_1)$ and $p_a = \delta(a - a_1)$]. Our approach for dealing with this is to interpret the ϵ and a in what follows as their mean values $\langle\epsilon\rangle$ and $\langle a\rangle$ if there is a range of ϵ and a present in our samples. Finally, for convenience, we will limit this percolation model to isotropic crack distributions.

A schematic of the model is shown in Fig. 2. Mathematically, our model for the overall isotropic rock conductivity σ_R in the absence of surface conduction (c.f., Section 5.2) takes the following form:

$$\sigma_R(\phi_2) = \begin{cases} \sigma_{\rm low}(\phi_2) & \text{when } 0 \le \phi_2 < \tilde{\phi}_2 \\ \sigma_{\rm cr}(\phi_2) = \sigma_{\rm low}(\phi_2) + \sigma_f \gamma_p \left(\phi_2 - \tilde{\phi}_2\right)^t & \\ \qquad\qquad \text{when } \tilde{\phi}_2 \le \phi_2 < \phi_2^* & \\ \sigma_{\rm hi}(\phi_2) & \text{when } \phi_2 \ge \phi_2^*. \end{cases} \tag{87}$$

At low-enough crack concentrations, the cracks are isolated in the porous host material. Any of the three standard effective medium theories (Maxwell, self-consistent, and differential embedding) give identical results for the overall conductivity $\sigma_{\rm low}(\phi_2)$ to leading (linear) order in ϕ_2. At a critical crack porosity $\tilde{\phi}_2$, the randomly placed cracks will form a connected path through the system, and percolation theory is used to model the conductivity through a so-called "critical region" where the conductivity exponent t is a universal constant for all cracked rocks. The dimensionless proportionality constant γ_p is expected to be close to one. Finally, at still higher crack concentrations $\phi_2 > \phi_2^*$, the clusters have sufficiently merged with the backbone and deadends that we can use any of the three effective medium theories to add cracks by writing $\phi_2 = \phi_2^* + \delta\phi_2$ and developing a dilute model $\sigma(\delta\phi_2)$ for a volume fraction $\delta\phi_2$ of cracks embedded into a background of conductivity $\sigma_{\rm low}(\phi_2^*) + \sigma_f \gamma_p (\phi_2^* - \tilde{\phi}_2)^t$. The transitional crack porosity ϕ_2^* is obtained from the continuity condition that

$$\left.\frac{d\sigma_{\rm low}}{d\phi_2}\right|_{\phi_2=\phi_2^*} + t\sigma_f\gamma_p(\phi_2^* - \tilde{\phi}_2)^{t-1} = \left.\frac{d\sigma_{\rm hi}}{d\delta\phi_2}\right|_{\delta\phi_2=0}. \tag{88}$$

This condition assures a smooth transition from the critical region to the high-concentration region.

In the ideal way of developing a percolation model that is valid across the entire range ϕ_2 (e.g., Kirkpatrick 1973), one would use an effective medium theory to define $\sigma_{\rm hi}$ in the high embedded-volume-fraction limit $\phi_2 \to 1$, which corresponds to the host "o" becoming the small volume-fraction embedded phase and the embedded phase "2" becoming the host phase. This would give $\sigma_{\rm hi}(\phi_2)$ valid as $\phi_2 \to 1$. One would then find the two constants γ_p and ϕ_2^* from the condition (88) and from

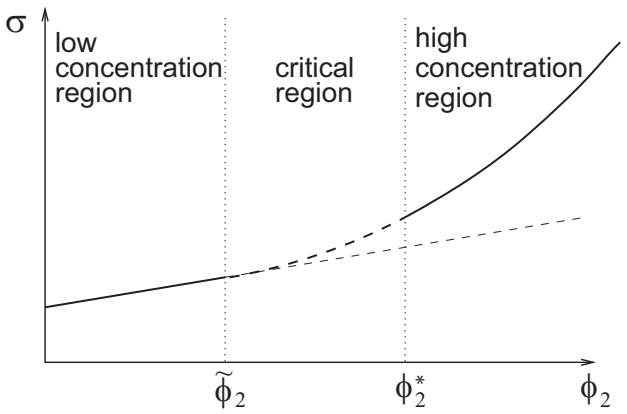

Figure 2 Schematic of the conductivity model. In the low-concentration region, the cracks do not overlap, and the conductivity varies linearly with crack porosity ϕ_2. Any of the standard effective medium theories give identical results in this region. At a critical crack porosity $\tilde{\phi}_2$, the cracks form a connected path across the sample, and percolation theory applies. In the high-concentration region, an effective medium theory is used to model the conductivity in the range $\phi_2 \ge \phi_2^*$.

the additional constraint that when $\phi_2 = \phi_2^*$, one has

$$\sigma_{\rm low}(\phi_2^*) + \sigma_f \gamma_p (\phi_2^* - \tilde{\phi}_2)^t = \sigma_{\rm hi}(\phi_2^*). \tag{89}$$

However, the $\phi_2 \to 1$ limit is difficult to define or even imagine (cracks occupying the entire sample); thus, we prefer to take $\gamma_p = 1$ in what follows and use only equation (88) to determine ϕ_2^*.

It is convenient to normalise the electrical conductivity by the fluid conductivity $\sigma_R = \sigma_f G$ and determine the inverse formation factor $G = 1/F$.

At low concentrations, we model $G_{\rm low}(\phi_2)$ using the coherent-potential approximation (e.g., Torquato 2002) for the effective conductivity of a porous host material having $G_o = \phi_o^m \ll 1$ with oblate ellipsoids having $G_2 = 1$ dilutely embedded in it. The coherent potential approximation for inverse formation factor $G_{\rm low}$ yields

$$(1-\phi_2)(G_{\rm low} - G_o) + \phi_2 (G_{\rm low} - 1) R^{(2o)} = 0. \tag{90}$$

Throughout what follows, we will need the so-called concentration parameter $R^{(2h)}$ for an embedded phase 2 placed in a host phase h.

For a uniform electric field $\mathbf{E}_o$ applied at infinity to a host (phase h) containing a single embedded ellipsoid (phase 2) with axis of revolution in the $\mathbf{E}_o$ direction, the electric field $\mathbf{E}$ inside the ellipsoid is uniform and given by $\mathbf{E} = \mathbf{R}^{(2h)} \cdot \mathbf{E}_o$, where (e.g., Stratton 1941)

$$\mathbf{R}^{(2h)} = \left[\begin{pmatrix} 1 & 0 & 0 \\ 0 & 1 & 0 \\ 0 & 0 & 1 \end{pmatrix} + \frac{(G_2 - G_h)}{G_h} \begin{pmatrix} Q & 0 & 0 \\ 0 & Q & 0 \\ 0 & 0 & 1-2Q \end{pmatrix} \right]^{-1}. \tag{91}$$

For oblate ellipsoids having minor axis $b = w/2$ (where w is the crack aperture) and major axis a (where a is crack radius) and $b/a < 1$, the shape factor Q is given by

$$Q = \frac{1}{2}\left[1 + \frac{1}{(b/a)^2 - 1} \left(1 - \frac{\tan^{-1}\sqrt{(a/b)^2 - 1}}{\sqrt{(a/b)^2 - 1}} \right) \right], \tag{92}$$

which for $b/a \ll 1$ (penny-shaped cracks) reduces to

$$Q = \frac{\pi}{4}\frac{b}{a}. \tag{93}$$

For the isotropic rock models we are developing in this paper, we then have that the concentration parameter $R^{(2h)}$ is

$$\begin{aligned} R^{(2h)} &= \frac{{\rm tr}(\mathbf{R}^{(2h)})}{3} \\ &= \frac{1}{3}\left[\frac{2G_h}{(1-Q)G_h + QG_2} + \frac{G_h}{2QG_h + (1-2Q)G_2} \right]. \end{aligned} \tag{94}$$

In this expression for $R^{(2h)}$, no assumptions have been made about the relative sizes of $G_{\rm low}$ and G_h as compared with the crack phase $G_2 = 1$ or to Q.

Returning to the low-concentration limit, we then have that with $G_2 = 1$ and $G_h = G_o = \phi_o^m \ll 1$, the leading order result in ϕ_2 becomes

$$G_{\rm low}(\phi_2) = G_o + (1 - G_o)\frac{2}{3}\frac{[1 + (G_o + Q)/2]}{(1 + Q/G_o)}\phi_2, \tag{95}$$

where we used the result

$$\begin{aligned} R^{(2o)} &= \frac{1}{3}\left[\frac{2G_o}{(1-Q)G_o + Q} + \frac{G_o}{2QG_o + 1 - 2Q} \right] && (96) \\ &= \frac{2}{3(1 + Q/G_o)}\left(1 + \frac{(G_o + Q)}{2}[1 + O(Q)] \right) \\ &\quad \times [1 + O(QG_o)] && (97) \\ &\approx \frac{2}{3(1 + Q/G_o)}\left(1 + \frac{(G_o + Q)}{2} \right). && (98) \end{aligned}$$

Here, we are assuming that $G_o \ll 1$ and $Q \ll 1$. Typically, for most materials of interest, we will have $Q < G_o$ but not hugely so. Note that it is through $Q = \pi b/(4a) = \pi \langle \epsilon(P_e) \rangle / 4$ that the effective pressure dependence of the electrical conductivity (formation factor) is modelled.

Comparing equations (95) and (86), we can identify the parameter ν_G more precisely as

$$\nu_G = \frac{1 + Q/G_o}{(1 - G_o)[1 + (G_o + Q)/2]}. \tag{99}$$

Whenever $Q \ll G_o \ll 1$, which is commonly the case, we have $\nu_G \to 1$ from above. Because the dilute limit of equation (95) is independent of the type of effective medium theory employed, equation (99) for the parameter ν_G can be considered generally valid for penny-shaped cracks.

The inverse formation factor in the critical region $\tilde{\phi}_2 < \phi_2 < \phi_2^*$ is given by (with $\gamma_p = 1$)

$$G_{\rm cr} = G_o + (1 - G_o)\frac{2}{3}\frac{[1 + (G_o + Q)/2]}{(1 + Q/G_o)}\phi_2 + \left(\phi_2 - \tilde{\phi}_2\right)^t. \tag{100}$$

To obtain the percolation threshold $\tilde{\phi}_2$, Garboczi *et al.* (1995) place oblate spheroids at random positions inside an insulating host (allowing for cracks to intersect) and numerically find that when $b/a < 10^{-3}$ (which is our "penny-shaped" regime of interest), the percolation threshold is

$$\tilde{\phi}_2 = 1.27\frac{b}{a}. \tag{101}$$

In a more recent study, Yi and Tawerghi (2009) perform a similar numerical study and find the percolation threshold

to be $\tilde{\phi}_2 = (0.9614 \pm 0.0005)b/a$. No reason for the discrepancy between the 1.27 and 0.96 factors has been suggested in the literature; however, for our purposes, simply taking the percolation threshold to be $\tilde{\phi}_2 \approx b/a$ makes no discernible difference in the final modeled results.

The total volume fraction η_2 of all embedded objects is

$$\eta_2 = v_2 \frac{N}{V}, \tag{102}$$

where v_2 is the volume of each inclusion and N is the total number of inclusions embedded in a volume V. The actual embedded porosity ϕ_2 allows for the randomly placed inclusions to overlap. The relation between the two is (Garboczi *et al.* 1991)

$$\phi_2 = 1 - \mathrm{e}^{-\eta_2}. \tag{103}$$

The relation between crack density ρ_c and crack porosity ϕ_2 when cracks can overlap is then (note that $v_2 = 4\pi ba^2/3$ so that $\eta_2 = 4\pi b\rho_c/(3a)$)

$$\rho_c = -\frac{3a}{4\pi b}\ln(1-\phi_2), \tag{104}$$

which reduces to the earlier statement (61) when $\phi_2 \ll 1$ (which is always the case). We thus find that the critical crack density for the percolation of penny-shaped cracks is

$$\tilde{\rho}_c = -\frac{3a}{4\pi b}\ln(1-b/a) \approx \frac{3}{4\pi} = 0.24, \tag{105}$$

although we continue to formulate the inverse formation factor in terms of crack porosity.

In the high-concentration regime, we are embedding cracks into a background host having inverse formation factor $G_{\mathrm{cr}}(\phi_2^*)$. The total crack porosity in this regime is $\phi_2 = \phi_2^* + \delta\phi_2$. Any of the three effective medium theories will give the same result for $G_{\mathrm{hi}}(\delta\phi_2)$ in the limit as $\delta\phi_2 \to 0$. In this limit, we have that

$$G_{\mathrm{hi}}(\delta\phi_2) = G_{\mathrm{cr}}(\phi_2^*) + s_m\,\delta\phi_2, \tag{106}$$

where

$$G_{\mathrm{cr}}(\phi_2^*) = G_o + s_o\phi_2^* + \left(\phi_2^* - \tilde{\phi}_2\right)^t, \tag{107}$$

and

$$s_o = [1 - G_o]\frac{2}{3}\frac{[1 + (G_o + Q)/2]}{[1 + Q/G_o]}, \tag{108}$$

$$s_m = [1 - G_{\mathrm{cr}}(\phi_2^*)]\,\frac{2}{3}\frac{[1 + (G_{\mathrm{cr}}(\phi_2^*) + Q)/2]}{\left[1 + Q/G_{\mathrm{cr}}(\phi_2^*)\right]}. \tag{109}$$

The transition probability ϕ_2^* physically corresponds to when enough crack clusters have linked to the initial backbone and dead-end clusters that connected cracks are rather uniformly spaced throughout the volume and effective-medium theory is again appropriate. This transition threshold is defined from the condition:

$$\left.\frac{dG_{\mathrm{hi}}}{d\delta\phi_2}\right|_{\delta\phi_2=0} = \left.\frac{dG_{\mathrm{cr}}}{d\phi_2}\right|_{\phi_2=\phi_2^*}, \tag{110}$$

which yields the implicit equation

$$s_o - s_m + t\left(\phi_2^* - \tilde{\phi}_2\right)^{t-1} = 0. \tag{111}$$

Due to the complicated dependence $s_m = s_m(\phi_2^*)$ given by equations (109) and (107), equation (111) is best solved numerically for ϕ_2^*. From the functional nature of $s_m(\phi_2^*)$, it is guaranteed that the solution of equation (111) always satisfies $\phi_2^* > \tilde{\phi}_2$. Finally, if ϕ_2^* is just slightly larger than the percolation threshold $\tilde{\phi}_2$, it may be of interest to define the high-crack-porosity limit using any one of the three standard effective medium theories (i.e., the Maxwell (or Mori-Tanaka), self-consistent (or coherent potential), and differential-embedding approximations) over larger ranges of the crack porosity where the conductivity is not just linear in the additional-crack porosity as assumed above. Torquato (2002) provides a convenient summary of the three effective medium theories for conductivity.

Bringing the model together, the rock conductivity is given by $\sigma_R = \sigma_f G = \sigma_f/F$, where the inverse formation factor $G = 1/F$ is given by

$$G(\phi_2) = \begin{cases} G_o + s_o\phi_2 & \text{when } 0 \le \phi_2 < \tilde{\phi}_2 \\ G_o + s_o\phi_2 + \left(\phi_2 - \tilde{\phi}_2\right)^t & \text{when } \tilde{\phi}_2 \le \phi_2 < \phi_2^* \\ G_o + s_o\phi_2^* + \left(\phi_2^* - \tilde{\phi}_2\right)^t + s_m(\phi_2 - \phi_2^*) & \\ \qquad\qquad \text{when } \phi_2 \ge \phi_2^*, \end{cases} \tag{112}$$

where s_o and s_m are given by equations (108) and (109), ϕ_2^* the solution of equation (111), $\tilde{\phi}_2 = b/a$, and G_o can be estimated from Archie's law to be $G_o = \phi_o^m$ (or from some other preferred means). To express these results in terms of the crack density ρ_c instead of the crack porosity ϕ_2, we use

$$\phi_2(P_e) = 1 - \exp\left(-\frac{4\pi\, b(P_e)\rho_c}{3a}\right) \approx \frac{4\pi}{3}\frac{b(P_e)}{a}\rho_c. \tag{113}$$

Finally, the half-aperture b varies with stress as $b(P_e) = w(P_e)/2 = b(0)\exp[-P_e/(\epsilon C_n)]$, where C_n is given by equation (26), and $\epsilon = b(0)/a$ is the aspect ratio at zero stress.

The earlier model for G of equation (86) is entirely equivalent to the low-crack porosity limit given by $G = G_o + s_o\phi_2$. For the non-linear percolation term in equation (112) to be negligible even at crack porosities above threshold, we need $G_o \gg (b/a)^2$, where we used $\tilde{\phi}_2 = b/a$ and $t = 2$. If $b/a = 10^{-3}$, then so long as $G_o \gg 10^{-6}$ (i.e., $F \ll 10^6$), which it most commonly will be, the earlier model of equation (86)

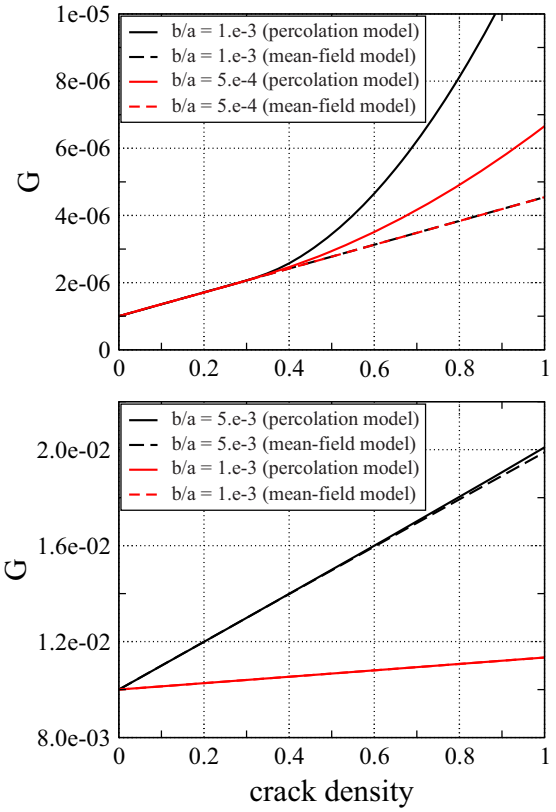

Figure 3 Inverse formation factor $G = 1/F$ as a function of crack density ρ_c for both a modelled crystalline rock with embedded cracks (upper panel) and a sandstone with embedded cracks (lower panel). The results called "mean-field model" correspond to equation (86), whereas those called "percolation model" correspond to equation (112). For the case of sandstones with large background (or host) conductivities, the percolating backbone of cracks has little influence on the overall conductivity. The thresholds $\tilde{\rho}_c$ and ρ_c^* are given in Table 1.

will be accurate even post percolation. This is simply saying that because the cracks are thin and because the crack-porosity backbone at percolation occupies such a small volume fraction and is rather tortuous, there is simply not enough current going through cracks compared with the conductive host for it to matter whether the cracks are connected or not.

In Fig. 3, we compare the estimates of G produced by equations (112) and (86). In the top panel of Fig. 3, we choose a very low level of background porosity $\phi_o = 10^{-3}$, which gives a background inverse formation factor of $G_o = 1/F_o = 10^{-6}$ (e.g., crystalline rock). One sees that, once the cracks percolate, the backbone makes a noticeable contribution to the rock conductivity. However, as seen in the lower panel, for a background porosity of $\phi_o = 10^{-1}$, which gives a background inverse formation factor of $G_o = 10^{-2}$

Table 1 Thresholds in the percolation conductivity models of Fig. 3

$\phi_o = 10^{-1}$ and $G_o = 10^{-2}$ (lower panel of Figure 3)

	$b/a = 5 \times 10^{-3}$	$b/a = 1 \times 10^{-3}$
$\tilde{\phi}_2$	6.375×10^{-3}	1.275×10^{-3}
$\tilde{\rho}_c$	0.3054	0.3046
ϕ_2^*	6.820×10^{-2}	8.193×10^{-3}
ρ_c^*	3.372	1.964

$\phi_o = 10^{-3}$ and $G_o = 10^{-6}$ (upper panel of Figure 3)

	$b/a = 5 \times 10^{-3}$	$b/a = 1 \times 10^{-3}$	$b/a = 5 \times 10^{-4}$
$\tilde{\phi}_2$	6.375×10^{-3}	1.275×10^{-3}	6.375×10^{-4}
$\tilde{\rho}_c$	0.3054	0.3046	0.3045
ϕ_2^*	0.3105	0.3139	0.3139
ρ_c^*	17.75	89.93	179.9

(sandstone), whether the cracks percolate or not makes little change compared with the background conductivity and background (non-percolating) embedded cracks. The pertinent thresholds in the percolation model are given in Table 1.

4.4 Percolation model for permeability

To make a percolation model for the permeability, it is sufficient to use the conductivity model above and insert $G_h = k_o$ for the conductivity of the host phase and $G_2 = b^2/3 = w^2/12$ for the conductivity of the embedded cracks. If we identify a dimensionless permeability

$$\kappa_o = 3k_o/b^2 \ll 1, \tag{114}$$

we can simply substitute κ_o for G_o in the conductivity model to obtain the permeability model

$$k(\phi_2) = \frac{b^2}{3}\begin{cases} \kappa_o + r_o\phi_2 & \text{when } 0 \le \phi_2 < \tilde{\phi}_2 \\ \kappa_o + r_o\phi_2 + \left(\phi_2 - \tilde{\phi}_2\right)^t & \text{when } \tilde{\phi}_2 \le \phi_2 < \phi_{2k}^* \\ \kappa_o + r_o\phi_{2k}^* + \left(\phi_{2k}^* - \tilde{\phi}_2\right)^t + r_m(\phi_2 - \phi_{2k}^*) & \\ & \text{when } \phi_2 \ge \phi_{2k}^*, \end{cases} \tag{115}$$

where r_o and r_m are obtained from equations (108) and (109) as

$$r_o = [1 - \kappa_o]\frac{2}{3}\frac{[1 + (\kappa_o + Q)/2]}{[1 + Q/\kappa_o]}, \tag{116}$$

$$r_m = \left[1 - \kappa_{\rm cr}(\phi_{2k}^*)\right]\frac{2}{3}\frac{[1 + (\kappa_{\rm cr}(\phi_{2k}^*) + Q)/2]}{\left[1 + Q/\kappa_{\rm cr}(\phi_{2k}^*)\right]}, \tag{117}$$

with

$$\kappa_{\rm cr}(\phi_{2k}^*) = \kappa_o + r_o\phi_{2k}^* + \left(\phi_{2k}^* - \tilde{\phi}_2\right)^t. \tag{118}$$

The transition probability ϕ_{2k}^* is numerically distinct from the conductivity threshold ϕ_2^* but again corresponds to when enough cracks have linked up to the backbone that a high-concentration limit can be defined using effective medium theory. It is obtained as the solution of the implicit equations

$$r_o - r_m + t\left(\phi_{2k}^* - \tilde{\phi}_2\right)^{t-1} = 0, \tag{119}$$

which, due to the complicated dependence $r_m = r_m(\phi_{2k}^*)$ given by equations (117) and (118), is best solved numerically. From the functional nature of $r_m(\phi_2^*)$, it is guaranteed that the solution of equation (119) always satisfies $\phi_{2k}^* > \tilde{\phi}_2$. To express these results in terms of the crack density ρ_c instead of the crack porosity ϕ_2, we again use equation (113).

For situations in which there is only a single value of ϵ and a throughout the crack population, the earlier model of equation (80) becomes $k = k_o + (2\phi_2 b^2)/(3\nu_k)$, which can be compared with the dilute limit of the percolation model $k_{\text{low}} = k_o + r_o\phi_2 b^2/3$ to yield

$$\nu_k = \frac{3(1 + Q/\kappa_o)}{(1 - \kappa_o)(1 + (\kappa_o + Q)/2}. \tag{120}$$

Under the common conditions where $Q \ll \kappa_o \ll 1$, we have $\nu_k = 3$ as anticipated.

The results of Fig. 3 directly translate to permeability if we identify the dimensionless parameter κ_o with G_o. As earlier, the percolation term is negligible in the percolation model whenever $\kappa_o \gg (b/a)^2$. For a low-permeability host having $k_o = 10^{-16}$ m^2 and if $b = \sqrt{3} \times 10^{-5}$ m, then $\kappa_o = 10^{-6}$ and the percolation results in the upper panel of Fig. 3 hold (exactly) after multiply by $b^2/3$. For a high-permeability host having $k_o = 10^{-12}$ m^2 and with $b = \sqrt{3} \times 10^{-5}$ m, then $\kappa_o = 10^{-2}$ and the results of the lower panel of Fig. 3 hold (exactly) after multiplying by $b^2/3$.

5 COMPARISON OF MODELLED GEOPHYSICAL PROPERTIES TO PUBLISHED DATA

The geophysical properties change during a brine injection experiment not only because the physical properties of the pore fluid are changing as a function of concentration C (mass of salt per mass of solution) and fluid pressure P but also because the pore space is deforming due to the applied stress $\boldsymbol{\tau}$ and fluid pressure P, as modelled above and primarily due to the presence of a crack population. Empirical correlations for the density and bulk modulus of a NaCl brine have been given by Batzle and Wang (1992), and we provide the needed formulas for the electrical conductivity of brine in Appendix.

Here, we summarise and use the models of the previous sections to predict how the P-wave velocity, S-wave velocity, electrical conductivity, porosity, and permeability are all changing due to either changing stress or fluid substitution. Unfortunately, there is no single published data set collected in a single laboratory where all of these properties have been measured on the same rock samples. In choosing published data to compare with, we choose datasets where more than one of these geophysical properties are being measured as a function of applied stress.

5.1 Seismic velocities

As a seismic wave propagates through the subsurface, it induces relative motion between the fluid and solid. The dimensionless number controlling whether viscous forces or inertial forces are resisting the relative flow is $\omega\rho_f k_o/\eta_f$ where ω is the circular frequency of the wave. Pride (2005) shows that, when $\omega\rho_f k_o/\eta_f \ll 1$, the poroelastic equations controlling P-wave propagation only involve undrained elastic moduli, and the response is, effectively, undrained (there is not enough time in each wave period for fluid to diffuse significantly from a compression toward a dilation due to the large wavelength). Therefore, when the wave frequency satisfies the inequality $f(= \omega/2\pi) \ll \eta_f/(2\pi k_o\rho_f) \approx 10^5$ Hz (assuming a 1 Darcy permeability which can be considered a large if not maximum value for consolidated rocks), the seismic response is undrained. Specialising to the case of isotropic rocks, the seismic velocities are thus given by

$$v_p(C, P, P_e) = \sqrt{\frac{K_u(K_f(C, P), P_e) + 4\mu(P_e)/3}{\rho_R(C, P)}}, \tag{121}$$

$$v_s(C, P, P_e) = \sqrt{\frac{\mu(P_e)}{\rho_R(C, P)}}, \tag{122}$$

where

$$\rho_R(C, P) = \phi_o\rho_f(C, P) + (1 - \phi_o)\rho_s. \tag{123}$$

Using these expressions for v_p and v_s, along with equations (52)–(53) and (6)–(7) that give $K_u(P_e)$ and $\mu(P_e)$, we can compare the modelled velocities as a function of P_e to those measured by Han *et al.* (1986). Four fitting parameters are required in the modelling: the elastic moduli of the host material K_{do} and μ_o, the aspect ratio of the cracks at zero effective stress $b(0)/a$ that is taken to be the same for all cracks in the fit, and the crack density ρ_c. In the data fitting, we did not allow K_{do} and μ_o to vary with stress.

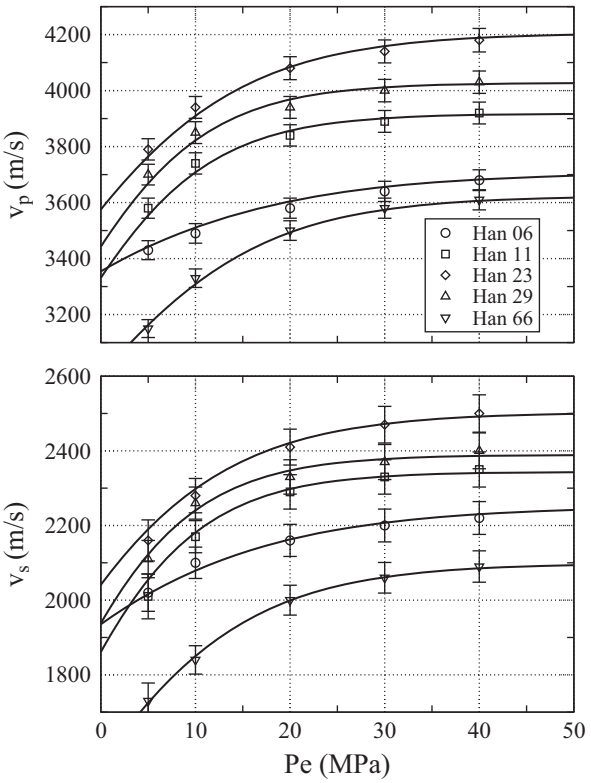

Figure 4 Solid lines are the theoretical predictions of this paper assuming a single aspect ratio is present, and symbols are the ultrasonic lab measurements of Han *et al.* (1986) on the five sandstone samples given in the legend. The four parameters used to obtain these fits for each rock sample are given in Table 2.

The results are shown in Fig. 4 with the parameters used to obtain the fits given in Table 2. The fits were done by eye and not optimised through least squares but are sufficient to demonstrate that the exponential stress dependence of a crack population, even with just a single aspect ratio present, can adequately explain the effective stress dependence of laboratory measured seismic velocities. Note that the high pressure results, where cracks are effectively closed, directly yield the elastic moduli of the host. The values of the host moduli as observed in the Han *et al.* (1986) sandstone data are entirely consistent with other measurements on sandstones (e.g., Castagna, Batzle, and Eastwood 1985). More perfect fits could have been obtained by introducing a broader range of aspect ratios, but Fig. 4 shows that a single aspect ratio captures most of the effective-pressure dependence of these consolidated sandstones.

Table 2 Parameters used to fit $v_P(P_e)$ and $v_s(P_e)$ sandstone data of Han *et al.* (1986). The values of porosity ϕ_o and percentage clay content were measured by Han *et al.* (1986). To the right of the vertical lines are the fit parameters used in the modelling of Fig. 4

Sample	ϕ_o	clay	$b(0)/a$	ρ_c	K_{do} (GPa)	μ_o (GPa)
Han06	0.24	0.10	4.8×10^{-4}	0.45	9.6	11.8
Han11	0.23	0.04	2.7×10^{-4}	0.85	13.4	12.8
Han23	0.19	0.05	2.4×10^{-4}	0.80	15.5	13.3
Han29	0.22	0.06	2.0×10^{-4}	0.80	15.5	13.3
Han66	0.27	0.06	3.5×10^{-4}	1.20	11.1	10.0

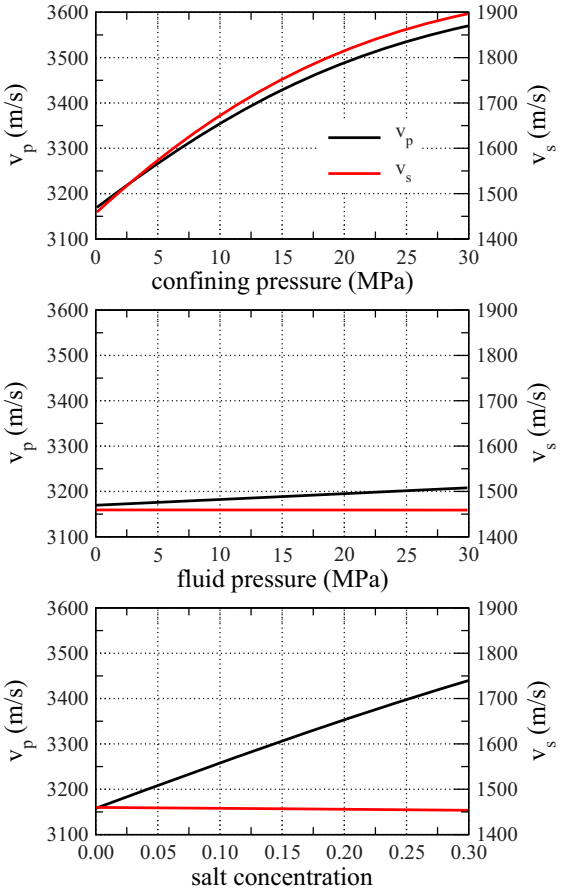

Figure 5 Variations of the undrained P-wave velocity (left axis, black curves) and S-wave velocity (right axis, red curves) for a simulated sandstone ($K_{do} = \mu_o = 30$ MPa, $\rho_c = 1$ and $b(0)/a = 5 \times 10^{-4}$) as a function of P_c, P, and C (mass of salt per mass of brine). In the top panel, the fluid pressure is kept constant at $P = 0.1$ MPa, and the salt concentration at $C = 0.05$ as the confining pressure P_c varies. In the middle panel, the effective pressure is kept constant at $P_e = 0$ MPa, and the salt concentration at $C = 0.05$ as the fluid pressure P varies. In the bottom panel, both the confining pressure and fluid pressure are kept constant at $P_c = P = 30$ MPa (so that $P_e = 0$), whereas salt concentration varies.

In Fig. 5, we simulate what happens to the seismic velocities of a simulated sandstone ($K_{do} = \mu_o = 10$ GPa with crack density $\rho_c = 1$ and single aspect ratio $b(0)/a = 5 \times 10^{-4}$) in

the following three scenarios: (i) the confining pressure P_c changes from 0.1 to 30 MPa, whereas fluid pressure $P = 0.1$ MPa and concentration $C = 0.05$ remain constant (upper panel); (ii) the fluid pressure P increases from 0.1 to 30 MPa, whereas the effective pressure $P_e = 0$ MPa and concentration $C = 0.05$ remain constant (middle panel); and (iii) the salt concentration increases from 0 to 0.3 (note that 0.3 is roughly the solubility limit of NaCl in water), whereas $P_c = P = 30$ MPa remain constant so that $P_e = 0$ (lower panel).

In the upper panel of Fig. 5, $v_p(P_c)$ and $v_s(P_c)$ are increasing for the sole reason that increasing $P_e = P_c - P$ is causing the crack compliance to decrease and the rock to stiffen. For this simulated rock, v_p increased by roughly 12% and v_s increased by 30% as P_e increased from 0 to 30 MPa.

In the middle panel, $P_e = 0$ is kept constant so that changes in crack compliance are not occurring. As the fluid pressure increases, the fluid bulk modulus increases and that is largely responsible for the observed 1.5% increase in $v_p(P)$ as P increases from 0.1 to 30 MPa. For $v_s(P)$, the only source of variation is the fluid density increasing with increasing P, and this effect is seen to be negligible over 0 to 30 MPa.

In the lower panel, we keep $P_e = 0$ (with $P_c = P = 30$ MPa) so that no changes to the crack compliances are occurring, and there are no fluid pressure variations of the fluid properties. The roughly 10% increase in v_p as C increase from 0 to 0.3 is due to how the bulk modulus of the fluid is increasing with C. The roughly 0.5% decrease in v_s with increasing C is due to how the fluid density is changing with C, and this effect can be considered negligible in a first approximation.

5.2 Electrical conductivity

Restricting attention to isotropic crack distributions, the general form for the isotropic electrical conductivity of rock σ_R is (e.g., Pride 1994)

$$\sigma_R(C, P, P_e) = G(P_e)\left[\sigma_f(C, P) + \frac{2C_s(C)}{\Lambda}\right]. \tag{124}$$

The first term corresponds to conduction through the pores of the host phase and cracks of the rock, whereas the second term corresponds to conduction over the solid surfaces in the rocks (so-called surface conduction).

In the surface conduction contribution, Λ is a length originally introduced by Johnson *et al.* (1986) that is a weighted pore volume to pore surface area ratio with the weight (the square of the dimensionless electric field in the porespace) emphasising constricted portions of the pore space, whereas the surface conductance C_s can have many contributing mechanisms, two of which are related to the presence of a diffuse double layer of excess ionic charge at the solid surfaces as defined and modeled by Pride (1994). Revil and Glover (1998) find that to fit shaly sandstone data, they need to allow for ionic conduction between the diffuse-double layer and the crystalline substrate in the so-called "Stern layer" of adsorbed water molecules and counter ions. They do not propose a physical model for why the adsorbed ions of the Stern layer are mobile and contributing to conduction, but such conduction, if it is occurring, makes a third contribution to the C_s term. In general, it is when significant amounts of secondary clay minerals are present on the detrital grains in sandstones, such that pore surface area is large and Λ small, that surface conduction becomes an important contributing factor to electrical conduction. This is the case in shaly sandstones. In the cracks, the crack surfaces are relatively smooth, and double-layer conduction is always negligible compared with conduction in the crack aperture (the width of the double layer is always negligible compared with the width of crack opening). Therefore, it is only in the host phase of shaly sandstones that surface conduction can be important.

The datasets where rock conductivity is a strong function of applied stress are those in which conduction is dominantly occurring through a connected crack population such as in crystalline rocks (e.g., granites). For such rocks, surface conduction can be neglected. We are not aware of a peer-reviewed dataset showing how the electrical conductivity of shaly sandstones varies with applied stress. As such, we will ignore surface conduction in this section and only focus on the first term of equation (124) where G (the inverse formation factor) is given by equation (85). However, if data warranted the inclusion of surface conduction, equation (124) makes clear how to do so.

The electrical conductivity of brine is given by (c.f., Appendix)

$$\sigma_f(C, P) = \frac{6.022 \times 10^{26} e^2}{6\pi\mu_{\text{salt}}}\left(\frac{\nu_+ z_+^2}{R_+} + \frac{\nu_- z_-^2}{R_-}\right)\frac{C\rho_f(C, P)}{\eta_f(C, P)}. \tag{125}$$

Here, μ_{salt} is the molecular mass of the salt measured in g/mol (see Appendix). For a NaCl brine that is the focus of this study, we then have

$$\sigma_f(C, P) = 2.17 \times 10^{-4}\frac{C\rho_f(C, P)}{\eta_f(C, P)}, \tag{126}$$

where the numerical prefactor and the fluid properties are all in SI units and where C is, as throughout, the salt concentration measured as a mass ratio.

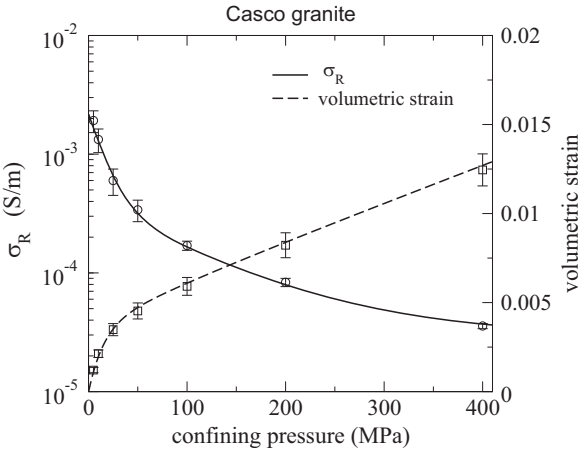

Figure 6 Electrical conductivity and volumetric strain of Casco granite as measured by Brace *et al.* (1965). The two aspect-ratio fits use the following parameters: $\epsilon_1 = 1.2 \times 10^{-4}$, $\epsilon_2 = 7.8 \times 10^{-4}$, $w_1 = 0.97$, $\phi_o = 3.2 \times 10^{-3}$, $\phi_2(0) = 3.0 \times 10^{-3}$, $C = 0.015$, and $K_{do} = \mu_o = 47$ GPa.

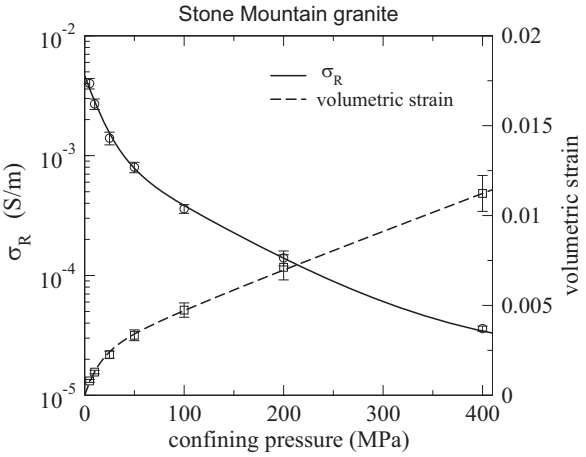

Figure 7 Electrical conductivity and volumetric strain of Stone-Mountain granite as measured by Brace *et al.* (1965). The two aspect-ratio fits use the following parameters: $\epsilon_1 = 1.2 \times 10^{-4}$, $\epsilon_2 = 7.0 \times 10^{-4}$, $w_1 = 0.95$, $\phi_o = 1.5 \times 10^{-3}$, $\phi_2(0) = 2.0 \times 10^{-3}$, $C = 0.05$, and $K_{do} = \mu_o = 47$ GPa.

In Figs. 6–8, the drained (constant fluid pressure) laboratory data of Brace *et al.* (1965) show how both electrical conductivity and volumetric strain of three different granite samples are changing with effective pressure. We model these data using equation (124) for the electrical conductivity and

$$\frac{\Delta V}{V}(P_e) = -\int_0^{P_e} \frac{dp}{K_d(p)}, \tag{127}$$

for the volumetric strain of the drained rock sample, where the effective stress dependence of the drained bulk modulus

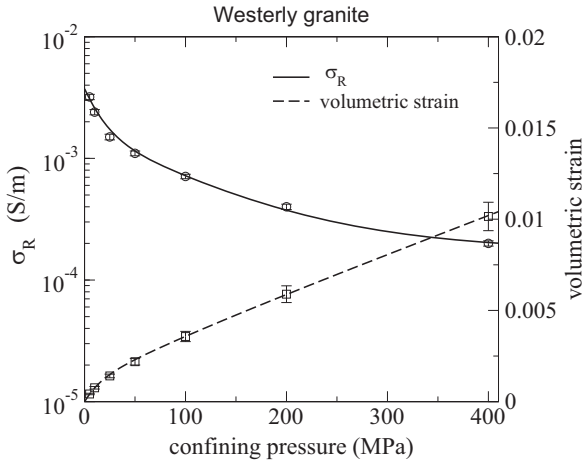

Figure 8 Electrical conductivity and volumetric strain of Westerly granite as measured by Brace *et al.* (1965). The two aspect-ratio fits use the following parameters: $\epsilon_1 = 1.2 \times 10^{-4}$, $\epsilon_2 = 7.7 \times 10^{-4}$, $w_1 = 0.9$, $\phi_o = 3.8 \times 10^{-3}$, $\phi_2(0) = 1.2 \times 10^{-3}$, $C = 0.065$ and $K_{do} = \mu_o = 47$ GPa.

of the cracked rock is modelled using equation (52). Due to the stiff nature of the background host granite, we did not model how the background host properties vary with P_e. For the probability distribution of aspect ratios, we found it necessary to use two aspect ratios in a three parameter distribution, i.e., $p_\epsilon(\epsilon) = w_1\delta(\epsilon - \epsilon_1) + (1 - w_1)\delta(\epsilon - \epsilon_2)$. Without using a second larger aspect ratio, we could never match the electrical conductivity measurement at 200 MPa. In the Westerly and Stone-Mountain granites, we found it necessary to use larger salt concentrations than the $C = 0.015$ solution that the samples were nominally saturated with. This might be due to these samples having some residual salt in the porespace prior to saturation. To eliminate fit parameters, we selected the drained moduli of the host to be $K_{do} = 47$ GPa and $\mu_o = 47$ GPa for all three granites.

5.3 Permeability and porosity

Finally, we consider the data of Zhu *et al.* (2002) where both permeability and porosity are measured on three sandstones (Berea, Adamswiller, and Rothbach) as confining pressure increases at constant fluid pressure. These authors are interested in the higher pressure regime where irreversible porespace collapse is resulting in large reductions of permeability and porosity; however, our interest is only in their lower pressure range of e.g., $P_e < 40$ MPa, where grain shattering is not occurring with increasing isotropic stress and prior to the application of shear stress.

To model isotropic permeability as a function of effective pressure, we use equation (80) when the crack porosity ϕ_2 is small relative to 1, i.e.,

$$k(P_e) = k_o(P_e) + \frac{8\pi}{9\nu_k}\rho_c \frac{\langle a^5\rangle}{\langle a^3\rangle}\int d\epsilon\; p_\epsilon(\epsilon)\epsilon^3 e^{-3P_e/(C_n\epsilon)}. \qquad (128)$$

The total porosity is changing with increasing confining pressure (note that, in the experiments, pore pressure is held constant) as

$$d\phi = -\left(\frac{(1-\phi)}{K_d(P_e)} - \frac{1}{K_s}\right) dP_c. \qquad (129)$$

This is integrated numerically starting from the known values at $P_c = P$. The host properties are allowed to change with increasing confining pressure according to the earlier derived results. The permeability and porosity of the host are determined from

$$\frac{dk_o}{k_o} = -\frac{[2\alpha_o/3 + m(\alpha_o - \phi_o)]}{\phi_o K_{do}} dP_c, \qquad (130)$$

and

$$d\phi_o = \frac{\left[(1-\phi_o)\rho_c f(P_e)4\pi/(3C_n) - (1-\phi_o)/K_d(P_e) + 1/K_s\right]}{1 - \rho_c\langle\epsilon(P_e)\rangle 4\pi/3} dP_c, \qquad (131)$$

again starting from the assumed known values at $P_c = P$. The drained modulus of the host is determined at each pressure increment from the model, i.e.,

$$K_{do} = \frac{K_s(1-\phi_o)}{1 + s_v\phi_o}, \qquad (132)$$

which then sets the Biot–Willis constant of the host

$$\alpha_o = 1 - \frac{K_{do}}{K_s}. \qquad (133)$$

We take the Archie exponent to be $m = 2$ and the bulk modulus of the solid grains to be $K_s = 40$ GPa.

In the fits to the Zhu, Montesi, and Wong (2002) data, we use only a single aspect ratio $\epsilon_1 = b(0)/a$ for each rock and a single crack radius a_1. The fit terms are then the crack density ρ_c, the aspect ratio ϵ_1, the crack radius a_1, the softness parameter s_v, and the permeability and porosity of the host rock at zero effective pressure $\phi_o(0)$ and $k_o(0)$.

The non-optimised fits are shown in Figs. 9–11. For effective isotropic stress larger than 40 MPa for example, there will be induced grain damage that is not being modeled in this paper. As such, we did not put an emphasis on modeling the data point at 60 MPa. If a second aspect ratio was used in modelling the data, the fits would necessarily have been better.

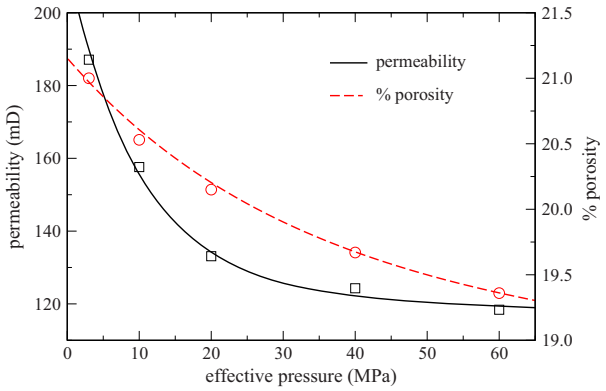

Figure 9 Single aspect-ratio fits to the permeability and porosity measurements of Zhu *et al.* (2002) for Berea sandstone. The non-optimised fit parameters are: $\rho_c = 4.2$, $\epsilon_1 = 8.6 \times 10^{-4}$, $a_1 = 6.0 \times 10^{-3}$ m, $s_v = 8.0$, $\phi_o(0) = 0.2117$, and $k_o(0) = 123$ mD.

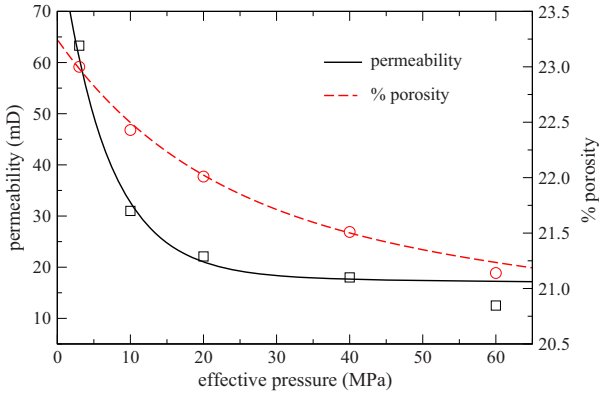

Figure 10 Single aspect-ratio fits to the permeability and porosity measurements of Zhu *et al.* (2002) for Adamswiller sandstone. The non-optimised fit parameters are: $\rho_c = 4.7$, $\epsilon_1 = 7.6 \times 10^{-4}$, $a_1 = 5.9 \times 10^{-3}$ m, $s_v = 11.0$, $\phi_o(0) = 0.2327$, and $k_o(0) = 18$ mD.

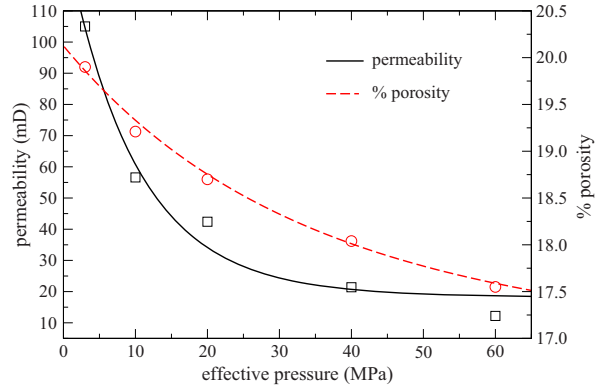

Figure 11 Single aspect-ratio fits to the permeability and porosity measurements of Zhu *et al.* (2002) for Rothbach sandstone. The non-optimised fit parameters are: $\rho_c = 6.0$, $\epsilon_1 = 8.6 \times 10^{-4}$, $a_1 = 5.7 \times 10^{-3}$ m, $s_v = 9.0$, $\phi_o(0) = 0.2015$ and $k_o(0) = 19$ mD.

6 CONCLUSIONS

In this paper, we provide models that describe how the elastic moduli, electrical conductivity, and fluid-flow permeability of rocks vary with effective stress. In order to fit laboratory-measured stress dependences of seismic velocities, porosity and permeability in sandstones, and volumetric strain and electrical conductivity in granites, we find it necessary to assume that a possibly porous host phase has a population of cracks embedded into it. Allowing for the porosity of the host phase alone to vary with stress without cracks present cannot explain the laboratory measurements. One of the central goals of this paper is to allow for the crack populations consistently in the effective-medium theory used to describe how the elastic moduli, electrical conductivity, porosity, and fluid-flow permeability vary with stress. For each modelled property, we first allow for the possibility that the crack population is anisotropic before specialising to the isotropic case for comparison to data on the sandstones and granites.

One feature of the mean-field theory used to obtain the explicit analytical forms for the elasticity, conductivity, and permeability tensors is that it does not matter where precisely the cracks reside inside a rock sample. All that matters is the density of cracks, the probability distribution for the crack aspect ratios and crack radii, and the averaged orientation of the cracks. In the mean-field theory employed here, the elastic compliance, conductivity, and permeability of a rock with a crack population are all linear in the crack density; their inverse, the elastic stiffness, electrical resistivity, and flow resistivity, are therefore non-linear in the crack density. The anisotropy of a rock with a crack population is controlled both by the averaged orientation of the cracks and, independently, by the presence or not of a deviatoric contribution to the stress tensor acting on a rock sample.

With regard to the transport properties of conductivity and permeability, the mean-field theory does not allow for the percolation effect of the cracks forming a connected path across the sample at sufficiently large crack density. We therefore provided a model for the transport properties that allows for the crack population to percolate. Using this model, it was demonstrated that for electrical conductivity, whenever the inverse formation factor $G_o = 1/F_o$ of the background host (where F_o is the formation factor of the host material) satisfies $G_o \gg (b/a)^2$, where b is a characteristic crack aperture and a a characteristic crack radius, the percolation effect is entirely negligible. Similarly, for permeability, when $3k_o/b^2 \gg (b/a)^2$, where k_o is the permeability of the host phase, the percolation effect is again negligible. Because the aspect ratios b/a needed to explain laboratory-measured stress dependence are typically on the order of 10^{-3} or less, the percolation effect is usually negligible. The exception can be in crystalline rocks in which the background host phase has very small conductivities and the crack phase significantly contributes to the transport. Even then, for the granites in the Brace *et al.* (1965) study that we modelled here, the percolation effect was again negligible due to the finite conductivity in the host phase. The host has to be effectively insulating before the percolation effect is important.

The models provided here are an attempt to obtain a consistent scheme for modelling how elasticity, conductivity, and permeability all vary with effective stress and the parameters describing a crack population. There are several "fit" parameters that can be adjusted to match laboratory data on the stress dependence of these properties. These include the properties of the background host phase (which are distinct for each modeled rock property) and the crack density, aspect-ratio distribution, and averaged crack orientations (which are common to all modelled rock properties). In looking at actual cracks and fractures in rocks, it is difficult to immediately see penny-shaped cracks. Actual cracks and fractures have a more bifurcated, jagged, and complex look to them compared with a random population of penny-shaped cracks. It is possible that the contribution of an actual fracture to the rock properties of a sample is equivalent to the sum of a bunch of properly oriented penny-shaped cracks and that our proposed models are doing a realistic job of representing the actual physics inside a sample. It is also possible that our effective medium theories simply provide a small number of tunable crack parameters that can describe laboratory data and that if actual crack densities and aspect ratios were determined for a rock sample, they would be somewhat different than the values required by our models to fit the data. However, even if this is true, the general correlation of how compliances and conductivity increase with increasing damage level in a sample would be properly represented by our models and that a population of penny-shaped cracks is simply a convenient proxy for representing the actual damage inside a sample. It does seem incontrovertible that the only way to explain the observed stress dependence measured on most consolidated rock samples is for damage (compliant cracks and fractures) to be present inside the rocks.

List of Symbols

α Biot–Willis coefficient [unitless]
α_k permeability effective-stress coefficient [unitless]

α_{ij} auxilliary matrix in Gassmann relations [unitless]
β_t tangential compliance parameter [Pa^{-1}]
ℓ pore length [m]
ϵ crack aspect ratio [unitless]
η_2 total volume fraction of all embedded cracks [unitless]
η_f fluid/brine viscosity [Pa s]
γ_p prefactor in percolation conductivity model [unitless]
$\kappa_o = 3k_o/b^2$ dimensionless permeability of host [unitless]
Λ surface conductance length parameter [m]
μ shear modulus [Pa]
μ_{salt} molecular mass of salt [g mol^{-1}]
ν Poisson's ratio [unitless]
ν_G prefactor for inverse formation factor model [unitless]
ν_k prefactor in permeability model [unitless]
$\nu_{+,-}$ ionic valances [unitless]
ϕ porosity [unitless]
ϕ_a azimuthal crack orientation [radian]
ρ_c crack density [unitless]
ρ_R saturated rock density [kg m^{-3}]
σ_f fluid/brine conductivity [S/m]
σ_n crack closure stress parameter [Pa]
σ_R rock conductivity [S/m]
θ longtitudinal crack orientation [radian]
A solid angle [radian]
a crack radius [m]
B Skempton's coefficient [unitless]
$b = w/2$ crack half aperture [m]
$b_{+,-}$ ionic mobilities [m s^{-1} N^{-1}]
B_n normal crack compliance [m Pa^{-1}]
B_t tangential crack compliance [m Pa^{-1}]
B_t tangential crack compliance [m Pa^{-1}]
C salt concentration by mass [unitless]
C_k permeability compliance parameter [Pa^{-1}]
C_n crack closure modulus [Pa]
C_s surface conductance [S]
C_{ijkl} stiffness tensor [Pa]
c_{ij} crack orientation tensor for permeability [unitless]
d_{ij} crack orientation tensor for conductivity [unitless]
E Young's modulus [Pa]
e fundamental charge of an electron [C]
F formation factor [unitless]
f effective stress function for compliances [unitless]
$G = 1/F$ inverse formation factor [unitless]
G_{ij} inverse formation factor tensor [unitless]
g_{ij} crack orientation tensor for compliances [unitless]
h_{ijkl} crack orientation tensor for compliances [unitless]
k permeability [m^2]
K_d drained bulk modulus [Pa]
K_f fluid bulk modulus [Pa]
K_s solid bulk modulus [Pa]
K_u undrained bulk modulus [Pa]
k_{ij} permeability tensor [m^2]
M fluid storage coefficient [Pa]
m Archie's exponent [unitless]
N number of cracks in a sample/voxel [unitless]
N_{salt} number density of dissociated salt molecules [m^{-3}]
P fluid pressure [Pa]
p_a probability distribution for crack radius [m^{-1}]
$P_c = -\mathrm{tr}\{\boldsymbol{\tau}/3\}$ confining pressure [Pa]
$P_e = P_c - P$ effective pressure [Pa]
Q inclusion shape factor [unitless]
R inclusion concentration parameter [unitless]
r_o **and** r_s auxilliary parameters in permeability model [unitless]
$R_{+,-}$ effective ionic radii [m]
S_c surface area of a single crack c [m^2]
s_o **and** s_m auxilliary parameters in conductivity model [unitless]
s_s softeness parameter in shear modulus model [unitless]
s_v softness parameter in bulk modulus model [unitless]
S_{ijkl} compliance tensor [Pa^{-1}]
t conductivity percolation exponent [unitless]
V sample or voxel volume [m^3]
V_2 total crack volume in a voxel [m^3]
V_ϕ pore-space volume [m^3]
v_p **and** v_s P- and S-wave velocities [m s^{-1}]
V_q net fluid exchange volume [m^3]
w crack aperture [m]
$\mathbf{B}$ crack compliance tensor [m Pa^{-1}]
$\mathbf{I} = \delta_{ij}\hat{\mathbf{x}}_i\hat{\mathbf{x}}_j$ identity tensor [unitless]
$\mathbf{n} = n_i\hat{\mathbf{x}}_i$ normal vector to crack [unitless]
$\mathbf{q}$ Darcy velocity [m s^{-1}]
$\mathbf{u}$ solid displacement [m]
$\mathbf{v}$ solid velocity [m s^{-1}]
$\mathbf{v}_f$ local fluid velocity in a crack [m s^{-1}]
$\boldsymbol{\tau}$ stress tensor [Pa]
$\boldsymbol{\tau}_e = \boldsymbol{\tau} + P\mathbf{I}$ effective stress tensor [Pa]

ACKNOWLEDGEMENTS

This material is based upon work supported by the U.S. Department of Energy, Office of Science, Office of Basic Energy Sciences, Chemical Sciences, Geosciences, and Biosciences Division under Contract DE-AC02-05CH11231.

REFERENCES

Archie G. E. 1942. The electrical resistivity log as an aid in determining some reservoir characteristics. *Transactions of the AIME* **146**, 54–62.

Batzle M. and Wang Z. 1992. Seismic properties of pore fluids. *Geophysics* **57**, 1396–1408.

Benveniste Y. 1987. A new approach to the application of Mori—Tanaka theory in compositematerials. *Mechanics of Materials* **6**, 147–157.

Berryman J.G. 2016. Role of fluid injection in the evolution of fractured reservoirs. *International Journal of Engineering Science* **103**, 45–58.

Berryman J.G. and Berge P.A. 1996. Critique of two explicit schemes for estimating elastic properties of multiphase composites. *Mechanics of Materials* **22**, 149–164.

Biot M.A. 1956. Theory of propagation of elastic waves in a fluid-saturated porous solid. I. Low-frequency range. *The Journal of the Acoustical Society of America* **28**, 168–178.

Biot M.A. and Willis D.G. 1957. The elastic coefficients of the theory of consolidation. *Journal of Applied Mechanics* **24**, 594–601.

Brace W., Orange A. and Madden T. 1965. The effect of pressure on the electrical resistivity of water-saturated crystalline rocks. *Journal of Geophysical Research* **70**, 5669–5678.

Castagna J.P., Batzle M.L. and Eastwood R.L. 1985. Relationships between compressional-wave and shear-wave velocities in clastic silicate rocks. *Geophysics* **50**, 571–581.

Cheng C.H. and Toksöz M.N. 1979. Inversion of seismic velocities for the pore aspect ratio spectrum of a rock. *Journal of Geophysical Research* **84**, 7533–7543.

Daley T.M., Schoenberg M.A., Rutqvist J., and Nihei K.T. 2006. Fractured reservoirs: an analysis of coupled elastodynamic and permeability changes from pore-pressure variation. *Geophysics* **71**, O33–O41.

Fortin J., Sanchits S., Dresen G. and Guegen Y. 2009. Acoustic emissions monitoring during inelastic deformation of porous sandstone: comparison of three modes of deformation. *Pure and Applied Geophysics*.

Gangi A. F. 1978. Variation of whole and fractured porous rock permeability with confining pressure. *International Journal of Rock Mechanics and Mining Sciences & Geomechanics Abstracts* **15**, 249–257.

Garboczi E., Snyder K., Douglas J. and Thorpe M. 1995. Geometrical percolation threshold of overlapping ellipsoids. *Physical Review E* **52**, 819–828.

Garboczi E., Thorpe M., Devries M. and Day A. 1991. Universal conductivity curve for a plane containing random holes. *Physical Review A* **43**, 6473–6482.

Gassmann F. 1951. Über die Elastizität poröser medien. *Vierteljahrsschrift der Naturforschenden Gesellschaft in Zürich* **96**, 1–23.

Grechka V. and Kachanov M. 2006a. Effective elasticity of rocks with closely spaced and intersecting cracks. *Geophysics* **71**, D85–D91.

Grechka V. and Kachanov M. 2006b. Influence of crack shape on effective elasticity of fractured rocks. *Geophysics* **71**, D93–D105.

Han D., Nur A. and Morgan D. 1986. Effects of porosity and clay content on wave velocities in sandstones. *Geophysics* **51**, 2093–2107.

Johnson D.L., Koplik J. and Schwartz L.M. 1986. New pore-size parameter characterizing transport in porous media. *Physical Review Letters* **57**, 2564–2567.

Kaselow A. and Shapiro S.A. 2004. Stress sensitivity of elastic moduli and electrical resistivity in porous rocks. *Journal of Geophysics and Engineering* **1**, 1–11.

Kestin J., Khalifa E. and Correia R. 1981. Tables of the dynamic and kinematic viscosity of aqueous NaCl solutions in the temperature range 20–150°C and the pressure range 0.1–35 MPa. *Journal of Physical and Chemical Reference Data* **10**, 71–87.

Kestin J. and Shankland R. 1984. Viscosity of aqueous NaCl solutions in the temperature range 20–100°C and in the pressure range 0.1–30 MPa. *International Journal of Thermophysics* **5**, 241–263.

Kirkpatrick S. 1973. Percolation and conduction. *Reviews of Modern Physics* **45**, 574–588.

Liu H.-H., Rutqvist J. and Berryman J.G. 2009. On the relationship between stress and elastic strain for porous and fractured rocks. *International Journal of Rock Mechanics and Mining Sciences* **46**, 289–296.

Liu H.-H., Wei M.-Y. and Rutqvist J. 2013. Normal-stress dependence of fracture hydraulic properties including two-phase flow properties. *Hydrogeology Journal* **21**, 371–382.

Masson Y.J., Pride S.R. and Nihei K.T. 2006. Finite-difference modeling of Biot's poroelastic equations at seismic frequencies. *Journal of Geophysical Research* **111**, B10305.

Mori T. and Tanaka K. 1973. Average stress in matrix and average elastic energy of materials with misfitting inclusions. *Acta Metallurgica* **21**, 571–574.

Oda M. 1985. Permeability tensor for discontinuous rock mass. *Geotechnique* **35**, 483–495.

Paterson M.S. and Wong T.F. 2005. *Experimental Rock Deformation –The Brittle Field*. Springer.

Pride, S. 1994. Governing equations for the coupled electromagnetics and acoustics of porous media. *Physical Review B*, **50**, 15678–15696.

Pride S.R. 2005. Relationships between seismic and hydrological properties. In: *Hydrogeophysics*, pp. 253–291. Springer.

Pride S.R. and Berryman J. 2009. Goddard rattler-jamming mechanism for quantifying pressure dependence of elastic moduli of grain packs. *Acta Mechanica* **205**, 185–196.

Sayers C. and den Boer L. 2012. Characterizing production-induced anisotropy of fractured reservoirs having multiple fracture sets. *Geophysical Prospecting* **60**, 919–939.

Sayers C. and Kachanov M. 1995. Microcrack-induced elastic wave anisotropy of brittle rocks. *Journal of Geophysical Research* **100**, 4149–4156.

Schoenberg M. 2002. Time-dependent anisotropy induced by pore pressure variation in fractured rock. *Journal of Seismic Exploration* **11**, 83–105.

Stratton J.A. 1941. *Electromagnetic Theory*. McGraw-Hill.

Thompson A.H., Katz A.J. and Krohn C.E. 1987. The microgeometry and transport properties of sedimentary rock. *Advances in Physics* **36**, 625–694.

Torquato S. 2002. *Random Heterogeneous Materials*. Springer.

Walton K. 1987. The effective elastic moduli of a random packing of spheres. *Journal of the Mechanics and Physics of Solids* **35**, 213–226.

Wyble D.O. 1958. Effect of applied pressure on the conductivity, porosity and permeability of sandstones. *Journal of Petroleum Technology* **10**, 57–59.

Yi Y. and Tawerghi E. 2009. Geometric percolation thresholds of interpenetrating plates in threedimensional space. *Physical Review E* **79**(4), 041134.

Zhang Y., Sayers C. and Adachi J. 2009. The use of effective medium theories for seismic wave propagation and fluid flow in fractured reservoirs under applied stress. *Geophysical Journal International* **177**, 205–221.

Zhu W., Montesi G.J. and Wong T.-F. 2002. Effects of stress on the anisotropic development of permeability during mechanical compaction of porous sandstones. *Geological Society, London, Special Publications* **200**, 119–136.

Zimmerman R.W., Somerton W. and King M.S. 1986. Compressibility of porous rocks. *Journal of Geophysical Research* **91**, 12765–12777.

APPENDIX

ELECTRICAL CONDUCTIVITY OF BRINES

The concentration measure of salinity that is most naturally used in the physical modelling of solute transport is the mass ratio C, which is defined:

$$C = \frac{\text{mass of salt (solute)}}{\text{mass of salt solution (solute + solvent)}}. \tag{A-1}$$

The mass ratio is the default concentration measure we use throughout all of our work.

The basic formula for the electrical conductivity of an electrolyte is

$$\sigma_f = e^2 \left(\nu_+ z_+^2 b_+ + \nu_- z_-^2 b_-\right) N_{\text{salt}}, \tag{A-2}$$

where $e = 1.602 \times 10^{-19}$ C is the fundamental electric charge, $b_\pm$ are the mobilities of the cations (+) and anions (-) defined as the speed these ions move under the influence of a force divided by the force amplitude acting on them, and N_{salt} is the salt number density defined as the number of dissociated salt molecules in a m^3 of solution. The number density N_{salt} is related to the molarity M (moles of salt per litre of solution) as $N_{\text{salt}} = 1000\mathcal{N}_A M$ where $\mathcal{N}_A = 6.022 \times 10^{23}$ is Avogadro's number (the number of objects in a mole) and where the factor of 1000 converts the liters in molarity to m^3. We further have that the molarity is related to C by $M = \rho_f C/\mu_{\text{salt}}$ where the electrolyte mass density $\rho_f(C, P, T)$ is modelled by Batzle and Wang (1992) using empirical correlations. Here, μ_{salt} is the total atomic mass of solute ions measured in grams per mole and given by

$$\mu_{\text{salt}} = \nu_+ \mu_+ + \nu_+ \mu_+, \tag{A-3}$$

where μ_+ is the atomic mass of the cation in an undissolved salt molecule and μ_- is the atomic mass of the anion. These numbers can be read from the periodic table. The numbers ν_+ and ν_- are the number of cations and anions in each undissolved salt molecule. The above formulas assume that all the salt molecules are completely dissolved (a so-called strong electrolyte). For a NaCl electrolyte, we have $\mu_{\text{salt}} = 58.44$ g/mol. At last, we can relate N_{salt} to C as

$$N_{\text{salt}} = 1000\mathcal{N}_A \frac{\rho_f}{\mu_{\text{salt}}} C, \tag{A-4}$$

for use in equation (A-2).

The mobilities can be related to the solvent through which the ions electromigrate by the Einstein–Stokes model that models each ion as a sphere of radius $R_\pm$ moving through a continuum of the brine solution having viscosity η_f

$$b_\pm = \frac{1}{6\pi\eta_f R_\pm}. \tag{A-5}$$

The effective ionic radii that give the measured mobilities of various ions at 25 °C are given in Table A1. The usefulness of equation (A-5) is that it allows salt concentration, temperature, and pressure to influence the ionic mobilities and, therefore, electrical conductivity of the solution, through the solution's shear viscosity η_f.

The viscosity of a brine has a negligible linear dependence on fluid pressure P but is a strong function of temperature T and a moderate function of concentration C. The empirical correlation for the viscosity of a NaCl brine over the

Table A1 Effective ionic radii for a few common ions to be used in the Einstein–Stokes model of equation (A-5)

Ion	Effective Ionic Radius $R_\pm$
H^+	0.23×10^{-10} m
Li^+	2.12×10^{-10} m
Na^+	1.63×10^{-10} m
K^+	1.12×10^{-10} m
Ag^+	1.33×10^{-10} m
Mg^{+2}	3.08×10^{-10} m
OH^-	4.14×10^{-10} m
Cl^-	1.07×10^{-10} m
Br^-	1.05×10^{-10} m
NO_3^-	1.15×10^{-10} m
SO_4^{-2}	2.59×10^{-10} m

range $0 < C < 0.24$, $20^{\circ}\text{C} < T < 150^{\circ}\text{C}$, and $10^5\text{Pa} < P < 3.5 \times 10^7\text{Pa}$ is obtained to within 0.5% accuracy by Kestin and Shankland (1984) as

$$\eta_f(C, T, P) = \eta_o(C, T)\left[1 + \frac{\beta(C, T)P}{1000}\right], \tag{A-6}$$

where the hypothetical zero-pressure viscosity is given by

$$\eta_o(C, T) = \eta_W(20)10^{\{A(C)+[1+B(C)]S(T)\}}, \tag{A-7}$$

where $\eta_W(20) = 1.002 \times 10^{-3}$ Pa s is a constant. The concentration functions $A(C)$ and $B(C)$ are defined as

$$A(C) = \sum_{i=1}^{3} a_i m^i. \tag{A-8}$$

$$B(C) = \sum_{i=1}^{3} b_i m^i. \tag{A-9}$$

with m being the molality (moles of salt per kg of pure solvent) which for a NaCl solution is

$$m(C) = \frac{1000}{\mu_{\text{salt}}}\frac{C}{(1-C)} = 17.11\frac{C}{(1-C)}. \tag{A-10}$$

The temperature function $S(T)$ is given by

$$S(T) = \frac{\sum_{i=1}^{4}\alpha_i(20-T)^i}{(96+T)}. \tag{A-11}$$

Finally, the pressure coefficient $\beta(C, T)$ is modelled as

$$\beta(C, T) = [\zeta_o + \zeta_1 T - \beta_W(T)]\,\beta^*(C) + \beta_W(T) \tag{A-12}$$

where the coefficient for pure water β_W is given by

$$\beta_W(T) = \sum_{i=0}^{4}\beta_i T^i, \tag{A-13}$$

and the coefficient controlling the salinity dependence $\beta^*(C)$ is given by

$$\beta^*(C) = \sum_{i=1}^{3}\beta_i^*\left(\frac{m}{m_s(T)}\right)^i, \tag{A-14}$$

where the molal normalization factor $m_s(T)$ is given by

$$m_s(T) = \sum_{i=0}^{2} m_i T^i. \tag{A-15}$$

The various coefficients in this correlation for the solution viscosity are given in Table A2. Note that the factor of 1000 in equation (A-6) is missing in the paper of Kestin, Khalifa, and Correia (1981) but is needed in order for the pressure dependence to be as given in their tables and to be consistent with their experimentally observed pressure dependence. Kestin *et al.* (1981) also have errors in their equations (4) and (5) (their exponent "2" should in fact be an "i") and in their equation (10) (their "β_i" should in fact be "β_i^*").

Table A2 The various coefficients for the viscosity correlations of Kestin *et al.* (1981). First column contains the coefficients for the C and T dependence, whereas the second column contains those for the P dependence

$\alpha_1 = +1.2378$	$\beta_0 = -1.297$
$\alpha_2 = -1.303 \times 10^{-3}$	$\beta_1 = +5.74 \times 10^{-2}$
$\alpha_3 = +3.06 \times 10^{-6}$	$\beta_2 = -6.97 \times 10^{-4}$
$\alpha_4 = 2.55 \times 10^{-8}$	$\beta_3 = +4.47 \times 10^{-6}$
$\eta_W(20) = 1.002 \times 10^{-3}$	$\beta_4 = -1.05 \times 10^{-8}$
$a_1 = +3.324 \times 10^{-2}$	$m_0 = +6.044$
$a_2 = +3.624 \times 10^{-3}$	$m_1 = +2.8 \times 10^{-3}$
$a_3 = -1.879 \times 10^{-4}$	$m_2 = +3.6 \times 10^{-5}$
$b_1 = -3.96 \times 10^{-2}$	$\beta_1^* = +2.5$
$b_2 = +1.02 \times 10^{-2}$	$\beta_2^* = -2.0$
$b_2 = -7.02 \times 10^{-4}$	$\beta_3^* = +0.5$
	$\zeta_0 = 0.545$
	$\zeta_1 = 2.8 \times 10^{-3}$

The electrical conductivity of the brine solution σ_f of equation (A-2) can now be re-expressed as a function of C, P, and T as

$$\sigma_f(C, T, P) = c_o\frac{\rho_f(C, T, P)}{\eta_f(C, T)}C, \tag{A-16}$$

where $\rho_f(C, T, P)$ is given by Batzle and Wang (2002), $\eta_f(C, T)$ is given above by equation (A-6), and the constant c_o is defined

$$c_o = \frac{e^2}{6\pi}\frac{1000\mathcal{N}_A}{\mu_{\text{salt}}}\left(\frac{\nu_+ z_+^2}{R_+} + \frac{\nu_- z_-^2}{R_-}\right). \tag{A-17}$$

The weak pressure dependence is only coming through the mass density. In addition to the dependence on C, the brine conductivity σ_f also has strong temperature dependence through the brine viscosity but only weak (negligible) dependence on fluid pressure.